

COSMIC FLOW FROM 2MASS REDSHIFT SURVEY: THE ORIGIN OF CMB DIPOLE AND IMPLICATIONS FOR  $\Lambda$ CDM COSMOLOGYGUILHEM LAVAUX<sup>1,2</sup>, R. BRENT TULLY<sup>3</sup>, ROYA MOHAYAEI<sup>1</sup>, STÉPHANE COLOMBI<sup>1</sup>*Draft version February 2, 2022*

## ABSTRACT

We generate the peculiar velocity field for the 2MASS Redshift Survey (2MRS) catalog (Huchra et al. 2005) using an orbit-reconstruction algorithm. The reconstructed velocities of individual objects in 2MRS are well-correlated with the peculiar velocities obtained from high-precision observed distances within  $3,000 \text{ km s}^{-1}$ . We estimate the mean matter density to be  $\Omega_m = 0.31 \pm 0.05$  by comparing observed to reconstructed velocities in this volume. The reconstructed motion of the Local Group in the rest frame established by distances within  $3,000 \text{ km s}^{-1}$  agrees with the observed motion and is generated by fluctuations within this volume, in agreement with observations. Having tested our method against observed distances, we reconstruct the velocity field of 2MRS in successively larger radii, to study the problem of convergence towards the CMB dipole. We find that less than half of the amplitude of the CMB dipole is generated within a volume enclosing the Hydra-Centaurus-Norma supercluster at around  $40h^{-1} \text{ Mpc}$ . Although most of the amplitude of the CMB dipole seems to be recovered by  $120h^{-1} \text{ Mpc}$ , the direction does not agree and hence we observe no convergence up to this scale. Due to dominant superclusters such as Shapley or Horologium-Reticulum in the southern hemisphere at scales above  $120h^{-1} \text{ Mpc}$ , one might need to go well beyond  $200h^{-1} \text{ Mpc}$  to fully recover the dipole vector.

We develop a statistical model which allows us to estimate cosmological parameters from the reconstructed growth of convergence of the velocity of the Local Group towards the CMB dipole motion. For scales up to  $60h^{-1} \text{ Mpc}$ , assuming a Local Group velocity of  $627 \text{ km s}^{-1}$ , we estimate  $\Omega_m h^2 = 0.11 \pm 0.06$  and  $\sigma_8 = 0.9 \pm 0.4$ , in agreement with WMAP5 measurements at the  $1\text{-}\sigma$  level. However, for scales up to  $100h^{-1} \text{ Mpc}$ , we obtain  $\Omega_m h^2 = 0.08 \pm 0.03$  and  $\sigma_8 = 1.0 \pm 0.4$ , which agrees at the  $1$  to  $2\text{-}\sigma$  level with WMAP5 results.

*Subject headings:* dark matter — methods:analytical, numerical and observation

## 1. INTRODUCTION

The Cosmic Microwave Background (CMB) dipole indicates that our Local Group (LG) moves with a velocity of  $627 \pm 22 \text{ km s}^{-1}$  towards the direction  $l = 276^\circ$ ,  $b = 30^\circ$  in galactic coordinates. The first attempt at making a comparison between the dipole induced by the gravitational influence of structures in our Local Universe and the observed CMB dipole was made by Yahil et al. (1980) using the revised Shapley-Ames catalog and by Davis & Huchra (1982) with the CfA catalog. This initial attempt was followed by a great number of works (Yahil et al. 1986; Lynden-Bell et al. 1989; Rowan-Robinson et al. 1990; Strauss et al. 1992; Hudson 1993). More recently, this comparison has been made with the extended source catalog of the 2 Micron All-Sky Survey by Maller et al. (2003). These studies all agree within  $10\text{-}30^\circ$  with each other and with the observed direction of the CMB dipole. Nowadays, it is considered unlikely that the Hydra-Centaurus-Norma supercluster at around  $40h^{-1} \text{ Mpc}$  could be solely responsible for the dipole. A number of authors suggests that one has to go at least as far as the Shapley concentration at about  $150h^{-1} \text{ Mpc}$  in order to fully recover the dipole mo-

tion (Kocevski & Ebeling 2006, Plionis & Kolokotronis 1998, Branchini & Plionis 1996, Strauss et al. 1992 for gravity induced dipole, Scaramella et al. 1989, Hoffman et al. 2001 for POTENT analysis of the observed tidal field). However, due mainly to sparseness of data at very large distances, there is still no consensus on the depth of the convergence for the CMB dipole, as some authors argued for a quicker convergence (Erdoğdu et al. 2006a, Erdoğdu et al. 2006b, Lynden-Bell et al. 1989, Lavav 1987, Lahav et al. 1988, Strauss et al. 1992, Yahil et al. 1986 and Lahav et al. 1989). This problem is even more complicated by the fact that we do not know with a high precision the value of the linear bias for each of these surveys. This uncertainty gives some freedom on the interpretation of the apparent convergence of the velocity of the Local Group. For example, Rowan-Robinson et al. (2000) argued that we reached a convergence assuming a low value for the biasing whereas Hudson (1994) argued against with a higher value for the biasing.

The other approach of studying the convergence of the velocity of the Local Group is to use surveys of peculiar velocities of galaxies. Watkins et al. (2009) showed that all the recent surveys give consistently a large bulk flow on a  $100h^{-1} \text{ Mpc}$  scale. Only the data of Lauer & Postman (1994) still remains inconsistent. This seems to indicate that the gravity induced dipole should not have converged by  $100h^{-1} \text{ Mpc}$ .

The common approach to recovery of the CMB dipole has been to use linear theory to reconstruct the veloc-

<sup>1</sup> Institut d'Astrophysique de Paris, UMR 7095 CNRS/Université Pierre et Marie Curie, 98bis bd Arago, France

<sup>2</sup> University of Illinois, Department of Physics, 1110 W. Green St, Urbana, IL, USA

<sup>3</sup> Institute for Astronomy, Univ. of Hawaii, Honolulu, USA

ity field from redshift surveys (see *e.g.* Erdoğan et al. 2006a, 2006b; Kocevski & Ebeling 2006). Methods based on linear theory can suffer from inadequacy in dealing with large fluctuations such as the Hydra-Centaurus-Norma supercluster, the Perseus-Pisces supercluster and the Virgo cluster. These problems may be enhanced by the coupling with redshift space distortions. Contrary to Erdoğan et al. (2006b), we also test here our reconstructed velocity field against distance measurements.

Here, we apply the Lagrangian method, Monge-Ampère-Kantorovitch (MAK), of peculiar-velocity reconstruction to the 2-Micron All-Sky Redshift Survey (2MRS) catalog (Huchra 2000; Huchra et al. 2005; Erdoğan et al. 2006a; Erdoğan et al. 2006b) and produce a 3-dimensional map of the velocity field and study the Local Group velocity convergence. Compared to Erdoğan et al. (2006b), we account better for non-linear effects in peculiar velocities, though at the price of having to correct for redshift distortion. The method has been adapted to work directly with redshifts and allows us to go well beyond the linear theory into the non-linear regime. The method has been tested previously against simulations and mock catalogs and has been shown to reconstruct reliable peculiar velocities on scales above 4-5 Mpc (see Lavaux et al. 2008 and references therein). In addition, using this method we can directly generate the 3-components of the peculiar velocities and hence overcome projection effects.

The reconstructed velocities of the 2MRS galaxies are tested against observed peculiar velocities obtained from high-precision distance measurements within a  $3,000 \text{ km s}^{-1}$  (3k) radius (Tully et al. 2008). The reconstructed and observed velocities are well-correlated with small dispersion. We make an independent estimate of  $\Omega_m$  using this comparison which is in excellent agreement with the results obtained using WMAP5 (Dunkley et al. 2009). The second test consists of comparing the reconstructed velocity of the Local Group in the rest frame of the  $3,000 \text{ km s}^{-1}$  sample to the observed velocity. Our results show that the Local Group motion in the rest frame of  $3,000 \text{ km s}^{-1}$  is mostly generated within this volume, as indicated by the observations (Tully et al. 2008).

Having tested our method, we study the origin of the CMB dipole. We reconstruct the velocity field of 2MRS in successively larger radii in order to determine whether there is any trend of convergence towards the CMB dipole. Contrary to Erdoğan et al. (2006b) but more in agreement with Pike & Hudson (2005), we show that the depth of the convergence in 2MRS lies beyond  $120h^{-1}$  Mpc. Due to severe incompleteness of the 2MRS catalog beyond  $120h^{-1}$  Mpc, we can only put a lower-limit on the value of the convergence depth. Our method allows us to determine the rate at which the dipole is approached: less than 50% of the dipole amplitude is achieved at around the Hydra-Centaurus-Norma distance and at  $\sim 120h^{-1}$  Mpc we recover about 87% of the amplitude of the CMB dipole but with no evidence for convergence in direction. We then compare the rate of convergence that we measure to theoretical predictions given by  $\Lambda$ CDM and the linear theory. It appears that our results are in agreement with  $\Lambda$ CDM when we consider galaxies at distances lower than  $60h^{-1}$  Mpc. Our results deviate  $1\sigma$  to  $2\sigma$  from expectations of the cosmology of WMAP5 for reconstruction of larger radii. A

problem relative to the bulk flow on a  $100h^{-1}$  Mpc scale has also been noted recently by Watkins et al. (2009) and on a  $300h^{-1}$  Mpc scale by Kashlinsky et al. (2008). Watkins et al. (2009) show that, though the bulk flow found by Lauer & Postman (1994) is not in agreement with any other peculiar velocity survey so far, there does exist an excessively large bulk flow, whose amplitude and direction is compatible with our findings. In this analysis, the Local Group velocity was taken as a constraint for the conditional probability density function. We have made a parallel analysis by removing this constraint and studying the joint probability distribution function instead of the conditional probability distribution function. We have tested that weighing our likelihood analysis by the probability of occurrence of the velocity of the Local Group does not change our results.

This paper is organized as follows. In Section 2, we introduce the 2MRS catalog and the  $3,000 \text{ km s}^{-1}$  distance catalog and we describe the catalog that we make by combining these two. In Section 3, we describe our method of peculiar velocity reconstruction. In Section 4, we constrain the density parameter  $\Omega_m$  by comparing the reconstructed velocity field of 2MRS with the observed velocities obtained from measured distances within the  $3,000 \text{ km s}^{-1}$  volume. In Section 5, we study the reconstructed evolution of the velocity of the Local Group towards the CMB dipole. We then discuss, in Section 6.1, the compatibility of this growth with the cosmological parameters as given by WMAP5. We develop a Bayesian analysis in Section 6.2 which allows us to make an estimate of cosmological parameters using our measurement on the velocity of the Local Group in different rest frames. In Section 7 we conclude.

## 2. THE COMBINED CATALOG: 2MASS REDSHIFT CATALOG (2MRS) PLUS CATALOG OF DISTANCES WITHIN $3,000 \text{ km s}^{-1}$ (3K DISTANCE CATALOG)

The 2MRS (Huchra 2000; Huchra et al. 2005) is the most uniformly sampled all-sky redshift survey to date and its selection in the near infra-red reduces the impact of the zone of avoidance. The catalog is based on galaxy selection in the infra-red from the Two Micron All-Sky Survey (2MASS, Skrutskie et al. 2006). The  $K=11.25$  mag 2MRS is now complete and contains about 23,200 galaxies. 2MRS provides good coverage to a mean distance of  $60h^{-1}$  Mpc and becomes extremely sparse afterward.

We fill the zone of avoidance, which mainly extends over  $|b| < 5 - 10^\circ$ , by mirroring galaxies from the unmasked region (first mentioned in Lynden-Bell et al. 1989, see also Shaya et al. 1995 and Lavaux et al. 2008 for details). The mask has been chosen to cover the part of the sky within  $10^\circ$  of the galactic plane for galactic longitudes  $l < 30^\circ$  and  $l > 330^\circ$ , and within  $5^\circ$  of it for other galactic longitudes. That way, we avoid the deeply obscured region behind the galactic bulge, at the expense of losing, *e.g.*, the Ophiuchus supercluster. The fake galaxies are represented by red points in the top panel of Fig. 1. The kinematic fingers of god (Jackson 1972), associated with clusters, are compressed using the algorithm of Huchra & Geller (1982). We used a fiducial velocity  $V_F = 1000 \text{ km s}^{-1}$ ,  $V_0 = 350 \text{ km s}^{-1}$ ,  $D_0 = 0.41 h^{-1} \text{ Mpc}$ , which corresponds to detecting galaxy count overdensities of  $\delta n/\bar{n} \simeq 80$

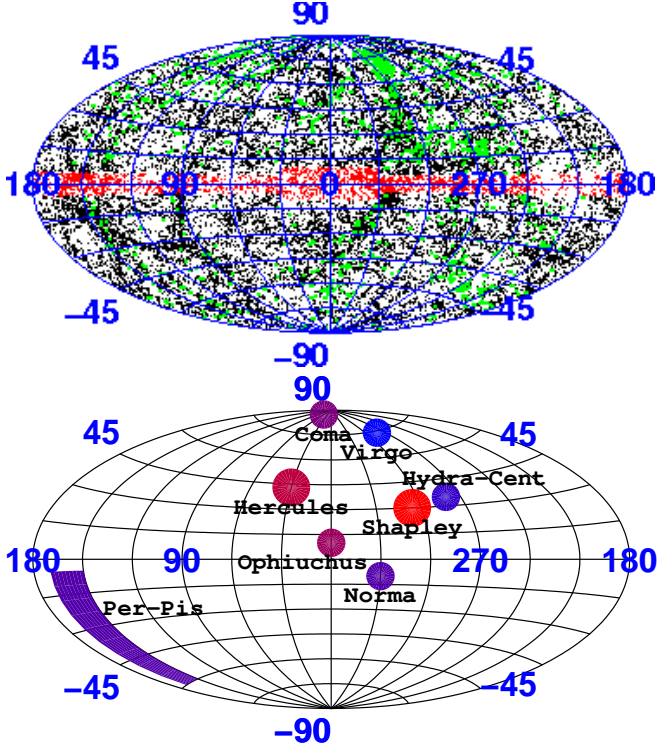


FIG. 1.— Combined 2MRS redshift catalog and 3k catalog of distances: Top panel: Large solid green circles are the galaxies for which a distance measure is available. The zone of avoidance has also been filled and is shown by the red belt running across the catalog. Bottom panel: angular positions of a few dominant superclusters in 2MRS catalog with more distant objects shown by redder circles. We represented the position of the Ophiuchus supercluster which has not been included in our galaxy sample.

(Crook et al. 2007, 2008) and provide robust statistical properties of groups as explained by Ramella et al. (1997). We assume a constant  $M/L$  ratio as it has been shown that the masses of big groups of galaxies only moderately depend on luminosities (Lin et al. 2004). Moreover, we have checked using the virial theorem on big groups of galaxies (typically  $M \gtrsim 10^{12} M_\odot$ ) that this is the best assumption we can make given the present data. Thus, for the calculation of the velocity of the Local Group, our method looks both like a flux-weighted computation (Lynden-Bell et al. 1989), because we depend on luminosities of galaxies to infer the mass, and number-weighted (Yahil et al. 1991), because we will be dependent on a correction of redshift distortions. Incompleteness is taken into account by using the Schechter luminosity function given in Crook et al. (2007) and Huchra et al. (2005) for 2MRS. The specific values of the parameters are:  $\Phi_* = 1.06 \cdot 10^{-2} h^3 \text{Mpc}^{-3}$ ,  $M_* = -24.2 + 5 \log_{10} h_{70}$ . We have verified that, as far as galaxies of the 2MRS are concerned, there does not seem to be any systematic effect in the relation between the  $K_{20}$  magnitude and the intrinsic luminosity.

We chose to execute the reconstruction itself in the CMB rest frame. Though it means that redshift distortions may be stronger near the observer, this ensures that better boundary conditions are enforced on the outer edge of the reconstruction volume. Using the

Local Group rest frame for large reconstruction volumes may lead to the equivalent of the so-called *rocket effect* (Kaiser 1987), which in the context of MAK still requires to be properly modeled. Being in the CMB rest frame, this effect should be negligible.

The second observational component is an extended catalog of galaxy distances. Information from four techniques has been integrated: the Cepheid variable (Freedman et al. 2001), Tip of the Red Giant Branch (Karachentsev et al. 2003; Lee et al. 1993), Surface Brightness Fluctuation (Tonry & Schneider 1988; Tonry et al. 2001), and Luminosity–Linewidth (Tully & Fisher 1977; Tully & Pierce 2000) methods. In all, there are 1791 galaxies with distance measures within  $3,000 \text{ km s}^{-1}$  (whence the name “3k catalog”); over 600 of these are derived by at least one of the first three ‘high quality’ techniques. The 3k catalog of distances has been described in detail by Tully et al. (2008).

The combined 2MRS catalog and 3k distance catalog are shown in Figure 1. In the present study, distances are averaged over groups because our method cannot meaningfully recover the velocities on sub-group scales. The present mixed catalog is composed of 24,819 galaxies, among which 1,126 has been assigned a distance. Distances are assigned to 109 groups of galaxies out of 695 groups. There are 617 galaxies with measured distances but which have not been grouped.

### 3. TECHNIQUE: MAK RECONSTRUCTION OF PECULIAR VELOCITY FIELD

The technique that will be implemented here is the Monge-Ampère-Kantorovich (MAK) reconstruction. This method provides a recipe for reconstructing galaxy orbits that is unique to the degree that orbits can be described as following straight lines under suitable co-ordinate transformations (Lavaux et al. 2008, and references therein). In essence, it tries to find the unique displacement field that does not produce shell crossings and that map an assumed homogeneous initial density field to the presently observed density field. Finding this displacement field corresponds to finding the solution of a Monge-Ampère equation, or to solve a Monge-Kantorovich problem (Brenier et al. 2003). This problem, once discretized, is equivalent to searching for the minimum of the discretized action

$$S = \sum_{i=1}^N \left( \mathbf{q}_{j(i)} - \mathbf{x}_i \right)^2. \quad (1)$$

which assigns initial comoving Lagrangian positions  $\mathbf{q}_j$  to final comoving Eulerian positions  $\mathbf{x}_i$ . We followed a different technique than in Lavaux et al. (2008) to account for redshift distortions. Modifying the action using Zel’dovich approximation may lead to quite large errors for the reconstruction of the velocity of the observer. In a volume of radius  $\sim 10 h^{-1} \text{ Mpc}$ , the distortions are dominant compared to the Hubble flow, and introduce extra shell crossings as compared to real space coordinates. We use a technique inspired from earlier attempt using linear theory (Pike & Hudson 2005). It consists in running an iterative algorithm on the smoothed reconstructed peculiar velocity field. The steps are as follows:

- (1) We let  $i$  be the iteration step number.



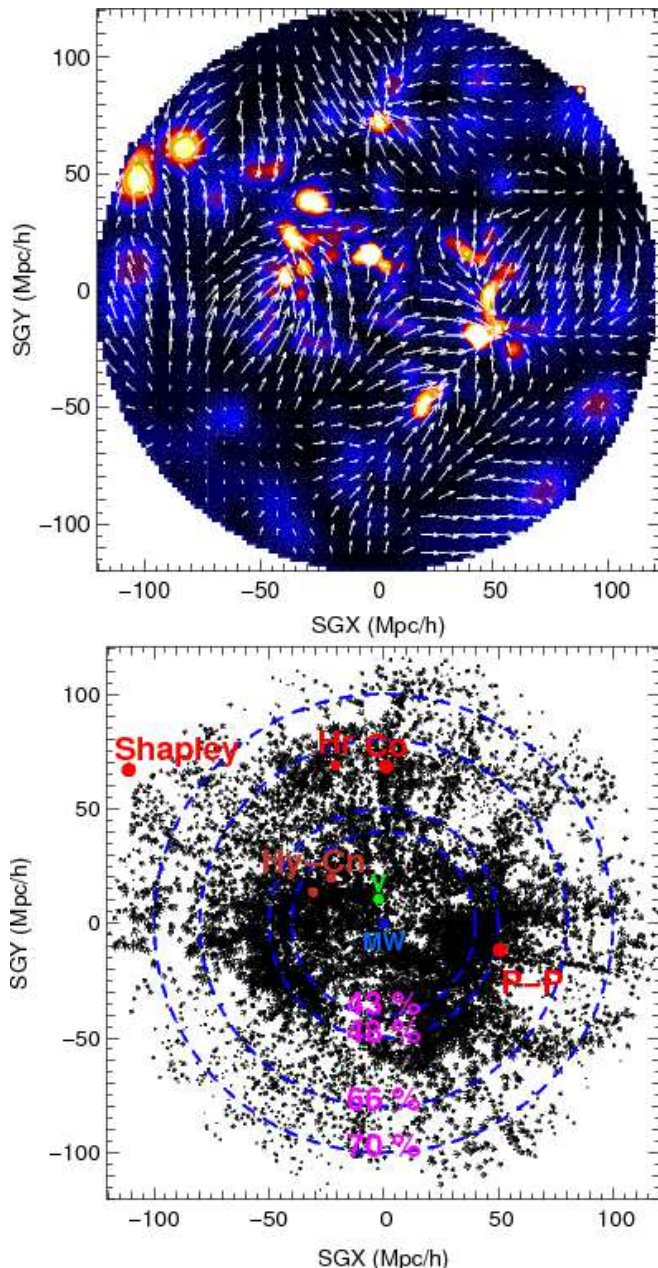


FIG. 2.— *2MRS peculiar velocity field*: Top panel shows a thin slice of the 2MRS peculiar velocity field adaptively smooth on a grid with  $128^3$  sites sampling a cube with an edge of  $240 h^{-1}$  Mpc. The velocity field is then subsampled 4 times before being shown. The underlying density field has been computed by putting objects at their redshift position. Bottom panel: Peculiar velocities of individual 2MRS galaxies in a  $40 h^{-1}$  Mpc slice, centered on the Supergalactic plane  $SGZ=0$  km s $^{-1}$ . 2MRS becomes severely incomplete after  $120 h^{-1}$  Mpc. Hy-Cn stands for the Hydra-Centaurus supercluster, Hr for Hercules, Co for Coma, P-P for Perseus-Pisces.

- (2) We run a reconstruction of the peculiar velocities on a catalog `Catalog(i)` of objects. The coordinates of these objects are assumed to be a good approximation of their real space coordinates. In that case we minimize the equation (1).
- (3) We smooth the reconstructed peculiar velocity in redshift space with a Gaussian kernel of radius

$2.5h^{-1}$  Mpc. This allows us to keep the large scale flow intact for the correction while alleviating the small scale effects for the correction of the distances of the objects of the catalog.

- (4) We move the objects back from their redshift coordinates from catalog `Catalog(0)` to their presumed new real space coordinates using the velocity field obtained at the step (3). This new set of position allows us to create the catalog `Catalog(i+1)` of objects.

- (5) We loop to point (1) until convergence.

We set `Catalog(0)` to be the 2MRS catalog in redshift coordinates. This algorithm in practice converges very quickly to the the true peculiar velocity field without redshift distortions, typically in 2 or 3 iterations. This effectiveness counterbalances the huge cost of running several MAK reconstruction.

#### 4. RESULTS: I. 2MRS VELOCITY FIELD AND COMPARISON WITH MEASURED DISTANCES: ESTIMATION OF $\Omega_M$

In reconstructing the velocity field using MAK based on priors, we first set  $\Omega_m = 0.258$  and bias (Kaiser & Lahav 1989) to 1 as indicated by WMAP5 results (Dunkley et al. 2009) and using 2dF and SDSS/WMAP results (Tegmark et al. 2004; Cole et al. 2005). We then do a self-consistency check on the presumed cosmological parameters by confronted reconstructed and observed Local Group motion. This is the approach taken in the next Section (Section 5). The velocity of each galaxy in 2MRS is reconstructed using these parameters and checked against observed distances within  $3,000$  km s $^{-1}$ . This test is detailed in Appendix D.

In this Section, we take a different approach and leave  $\Omega_m$  free and then constrain its value by maximizing the correlation between the reconstructed and observed peculiar velocities. This approach allows us to constrain the value of the bias parameter. The 2MRS velocities are reconstructed using a uniform grid of size  $130^3$  sampling a cubic volume of  $260^3 h^{-3} \text{Mpc}^3$  as shown in Fig. 2. The motion of the Local Group is obtained using an interpolation based on the adaptive weighting of the peculiar velocities of the objects that lie within  $4\text{--}5h^{-1}$  Mpc from us (method detailed in Appendix C). We have checked that increasing the reconstruction resolution does not significantly change the reconstructed velocities.

We present, in Fig. 3, the result of the comparison of observed peculiar velocity field vs. reconstructed peculiar velocity field in the volume of radius  $3,000$  km s $^{-1}$ . Both fields have been obtained using adaptive smoothed interpolation on the the line-of-sight component of the velocities (observed or reconstructed) of the objects put at their redshift position (Appendix C). As we are using the redshift coordinates, and not the distance-induced coordinates, we should be free of the so-called volume Malmquist bias. Moreover, the two fields are enforced to be smoothed in exactly the same way at each spatial location, the one needing a larger smoothing scale prevailing on the other. Finally, we opted for smoothed interpolation considering that galaxies are fair tracers of the underlying continuous velocity field. As it is adaptive, the smoothing scale is left free, while in practice it remains

in the range  $[3.4, 8.7]h^{-1}$  Mpc.<sup>4</sup> The top panel gives the result of the comparison of the raw velocities. However, it may happen that the bulk flow of the  $3,000 \text{ km s}^{-1}$  volume is badly reconstructed. To avoid this problem, we subtract the reconstructed (observed respectively) bulk velocity of the  $3,000 \text{ km s}^{-1}$  region from reconstructed (observed respectively) peculiar velocities. The comparison of the resulting fields is given in the bottom panel of Fig. 3. The observed and reconstructed velocities are now visually well-correlated. To test the correlation, we use two quantities already introduced in Lavaux et al. (2008). First, we define the correlation coefficient

$$r = \frac{\langle \tilde{v}_{\text{rec},r} \tilde{v}_{\text{obs},r} \rangle}{\sqrt{\langle \tilde{v}_{\text{rec},r}^2 \rangle \langle \tilde{v}_{\text{obs},r}^2 \rangle}} \quad (2)$$

with  $\tilde{v}_{\text{rec},r} = v_{\text{rec},r} - \langle v_{\text{rec},r} \rangle$  and  $\tilde{v}_{\text{obs},r} = v_{\text{obs},r} - \langle v_{\text{obs},r} \rangle$ ,  $v_{\text{rec},r}$  the line-of-sight component of the reconstructed velocity field,  $v_{\text{obs},r}$  the line-of-sight component of the observed velocity field. Second, we define the typical reconstruction error

$$\sigma^2 = \frac{1}{2} \langle (\tilde{v}_{\text{rec},r} - \tilde{v}_{\text{obs},r})^2 \rangle \quad (3)$$

We obtain  $r = 0.73$  and  $\sigma = 65 \text{ km s}^{-1}$ . These values show that our reconstructed velocity field is of good quality. Indeed, the standard deviation  $\sigma$  is rather small compared to the typical extent of the PDF ( $\sim 400 \text{ km s}^{-1}$ ). The correlation  $r$  is better than what has been obtained for mock catalogs for which observational effects have been included ( $r_{\text{mock}} \simeq 0.53$ ), in spite that the comparison is done on a smaller number of tracer of the peculiar velocity field: 576 tracers within  $3,000 \text{ km s}^{-1}$  in the case of this paper against  $\sim 1600$  in mock catalogs. This seems to indicate that our results should be as good as the one obtained on simulations (Lavaux et al. 2008).

From the comparison between reconstructed to observed peculiar velocities, it is possible to measure  $\Omega_m$ . Though a pure likelihood approach would seem the natural way, Lavaux et al. (2008) showed the high sensitivity to the prior of a likelihood which does not take into account correlations of the velocity field. For this paper, we will thus use the apparently less sensitive method of moments (Colombi et al. 2007; Lavaux et al. 2008) to determine  $\Omega_m$  on the adaptively smoothed velocity field. Smoothing has the advantage of using the correlation of the velocity field to increase the signal-to-noise. The noise coming from both errors on observed distances and from MAK modeling will be in particular diminished. As it has been shown in this paper that the slope between reconstructed displacements and observed peculiar velocities

$$s = \sqrt{\frac{\langle \tilde{v}_{\text{rec},r}^2 \rangle}{\langle \tilde{v}_{\text{obs},v}^2 \rangle}} \quad (4)$$

seems not to be statistically biased, we will use it here as our estimator of  $\Omega_m$ . We improve the technique by computing a set of different slopes from data points that lies farther and farther from the perfect correlation (i.e. the diagonal in Fig. 3). This allows us to make an estimate of the error bar on our result on  $\Omega_m$  through the

<sup>4</sup> This range corresponds to the selected smoothing radius for 95% of the volume.

use of the two other estimator of the slope  $r \times s$  and  $s/r$  (Appendix B of Lavaux et al. 2008).

We assumed  $h = 0.80$ , a value compatible with the catalog of distances with the current calibration of distance indicators. The value assumed for  $h$  only marginally affects our estimation of  $\Omega_m$  as it was shown in Lavaux et al. (2008). From the 576 velocities that were reconstructed, we estimate  $\Omega_m = 0.31 \pm 0.05$ . This result is in agreement with Pike & Hudson (2005). This is only consistent at the lower end of  $\Omega_m$  with previous results based on orbit reconstruction methods (e.g. Mohayaee & Tully 2005). An extensive likelihood analysis including correlations, which would yield a better estimation, is postponed to another paper.

We estimate a systematic error of  $\sim 9\%$  on reconstructed peculiar velocities due to the assumed values of cosmological parameters. To this error, we add in quadrature a random reconstruction error of  $70 \text{ km s}^{-1}$  according to the mean (both on amplitude and by component), as estimated using reconstruction on simulations in redshift space (Fig. 8, Appendix B).

One must be aware of the danger of cosmic variance, as it has been highlighted in Lavaux et al. (2008). A way of checking it is to use the density field of the whole 2MRS as an indicator of the local density fluctuation. We computed a density contrast  $\rho_{30}/\rho_{100} - 1 = -0.046$  for the Universe within  $30h^{-1}$  Mpc, compared to the mean density within  $100h^{-1}$  Mpc using the mass density field obtained from 2MRS data. It means the volume on which we make the comparison is slightly underdense and thus may bias our value to lower  $\Omega_m$ . However, the amount of the systematic bias due to cosmic variance seems to be here negligible compared to errors due solely to the noise. Nevertheless, this value is in good agreement with other measurements such as the one given by WMAP (Dunkley et al. 2009) for the  $\Lambda$ CDM model. Having obtained and tested our reconstructed velocities within  $3,000 \text{ km s}^{-1}$ , we go to larger scales and study the origin of the motion of the Local Group with respect to CMB,  $V_{\text{LG/CMB}}$ , in the next section.

## 5. RESULTS: II. 2MRS VELOCITY FIELD AND THE ORIGIN OF THE CMB DIPOLE

The CMB dipole motion, is obtained by using the reconstructed 3d velocity field generated using the 2MASS Redshift Survey. The velocities are reconstructed within increasing radii centered on the Local Group. A table of the resulting dipole as a function of the reconstruction radius is given in Table 1. The entries are represented in Fig. 4. No convergence is achieved below  $120h^{-1}$  Mpc. The 2MRS sample becomes highly incomplete beyond this scale and further conclusions cannot be made before a more complete sample becomes available. Whether the Shapley supercluster yields the convergence to the CMB dipole also remains questionable, as farther away in the southern hemisphere, dominant structures such as the Horologium-Reticulum supercluster could change the direction of the dipole. Thus, it is possible that the depth of the convergence towards CMB dipole lies well-beyond the Shapley concentration itself.

We also plot the increase in the bulk flow relative to the CMB dipole over the reconstructed peculiar velocities within  $120h^{-1}$  Mpc in the bottom panel of Fig. 2. The figure demonstrates that less than half of the am-

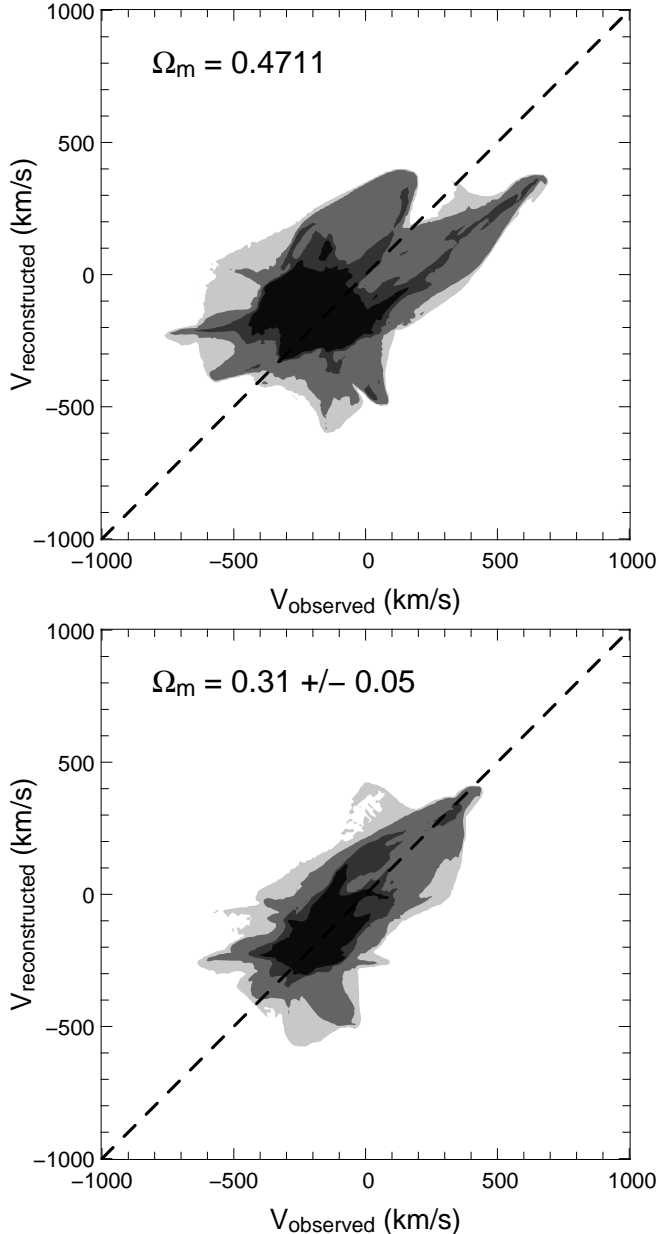


FIG. 3.— *Observed vs. Reconstructed velocity field* – These two panels give the result of the comparison between the reconstructed and the observed line-of-sight component of the velocity field. The top (respectively bottom) panel indicates the result of a comparison before (respectively after) having corrected for bulk flows. We have used the method of moments using the part of the scatter within the 95% probability contour in both cases. For the top panel we obtain  $\Omega_m \sim 0.47$ . For the bottom panel, we estimate  $\Omega_m \sim 0.31$ . The correlation coefficient  $r$  in that case is equal to 0.73, with a typical a posteriori velocity error of  $65 \text{ km s}^{-1}$ . To plot these two distributions, we assumed  $h = 0.80$ . Though the centroid of the scatter has been repositioned for the estimation of the slope, this correction has not been applied for the above distributions. Decreasing  $h$  would move the scatter to the right of the diagonal. The filled contours limit the regions that corresponds to 50% (black), 68% (dark gray), 95% (gray) and 99% (light gray) of joint probability to have a reconstructed and an observed velocity at some position in the Local Universe.

plitude of the dipole is generated within the volume enclosing Hydra-Centaurus-Norma. To reach convergence a significant contribution to the dipole has to be made from the Shapley supercluster and beyond. This agrees with an analysis of the X-ray data (Kocevski & Ebeling 2006). We also fail to observe convergence by the time we reach  $120h^{-1} \text{ Mpc}$ . Indeed, although the amplitude of the reconstructed dipole seems to approach that of CMB, its direction remains well away from it. Using observational error bars, we estimate that the observational error on the direction of the Local Group velocity should not exceed  $\sim 6^\circ$  at 95% confidence. In addition, we estimated from an  $N$ -body  $\Lambda$ CDM simulation that there is an intrinsic  $22^\circ$  error (95% confidence) in the direction of the reconstructed velocity because of the modeling errors of the MAK reconstruction. In sum, we expect the observed and reconstructed vectors to agree to within  $\sim 23^\circ$  whereas they lie at  $\sim 40 - 50^\circ$  from each other. This problem is highlighted by Fig. 5, where we have represented the angular separation between the reconstructed Local Group velocity and the CMB dipole. We note that beyond  $\sim 60h^{-1} \text{ Mpc}$  the separation remains at roughly  $40 - 50^\circ$ . We now proceed to compare our results to predictions given by the  $\Lambda$ CDM model.

#### 6. COMPATIBILITY WITH THE $\Lambda$ CDM MODEL

The measurements of the convergence of the velocity of the Local Group to the CMB dipole can be used to check the  $\Lambda$ CDM model. Indeed, the statistic of peaks and voids in the density field imprints the fluctuation and the rate at which the velocity of the Local Group converges to its expected final value, which should be the one given by the CMB according to the current cosmological paradigm. We will use here the cosmological parameters estimated by WMAP5 (Dunkley et al. 2009) and weak lensing measurements (Fu et al. 2008; Benjamin et al. 2007; Massey et al. 2007). We use a statistical modeling of the Local Group velocity growth developed by Juszkiewicz et al. (1990) (equation 12) and Lahav et al. (1990). The prediction is based on linear theory and is able to give the probability of occurrence of our measurements given the cosmological model. As proposed by Dunkley et al. (2009) and Fu et al. (2008), we use  $\Omega_m = 0.256$  (the density of baryon is  $\Omega_b = 0.044$  and the density of cold dark matter is  $\Omega_c = 0.212$ ) and  $\sigma_8 = 0.77$ . We also set the Hubble constant to  $H = 71.9 \text{ km s}^{-1} \text{ Mpc}^{-1}$  and the spectral index  $n = 1$ . In addition to the cosmology specified above, we enforce that the amplitude of the velocity of the Local Group is  $627 \text{ km s}^{-1}$ .

This conditioning allows us to avoid the problem of the probability of our own velocity in the different universes we consider in this work. Thus, though we may be at a special point in the Universe, our results should not be affected by the fact that the velocity of Local Group may be unusual. In the following, we thus focus on the conditional probability of obtaining a set of reconstructed velocities of the local group  $\{\mathbf{v}_i\}$  given a specification of the velocity of the Local Group  $\mathbf{V}_{\text{LG}}$ . Nevertheless, we have also checked in Section 6.2 that using the joint probability of having both  $\{\mathbf{v}_i\}$  and  $\mathbf{V}_{\text{LG}}$  only slightly changes the probability contours in the specific case of our velocity as given in Table 1. This indicates that the velocity of the Local Group is not too uncommon in



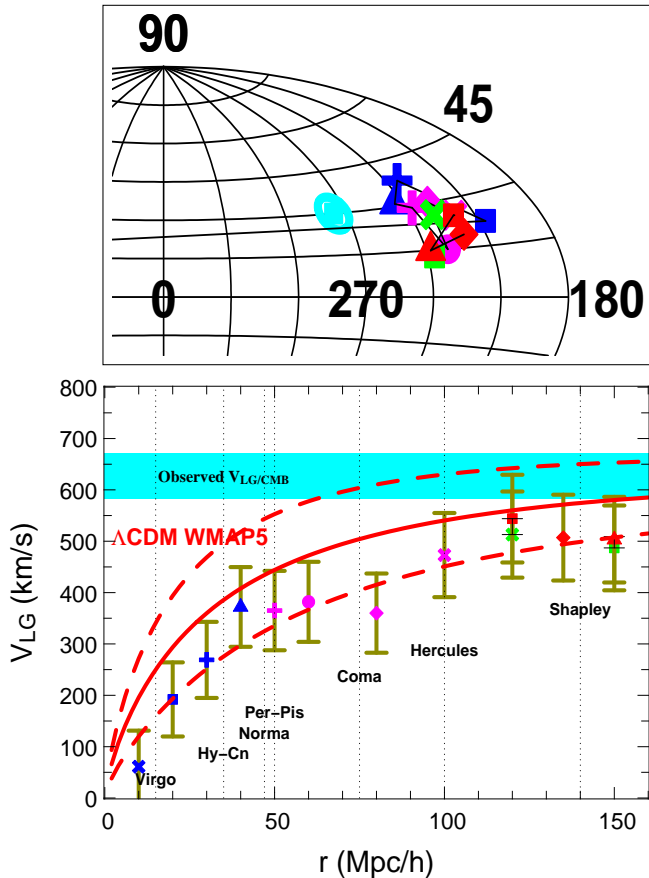


FIG. 4.— *Velocity of the Local Group in progressively larger rest frames,  $V_{LG}$* : The observed amplitude and direction of the CMB dipole motion are shown by the horizontal cyan band in the lower panel and the solid cyan large square in the top panel, respectively. The lower panel shows the amplitude of the velocity of the Local Group in successively larger rest frames as the velocity field of 2MRS is reconstructed at increasing radii. Incompleteness is illustrated by the black error bar on data points beyond  $120h^{-1}$  Mpc in the bottom panel. The top panel shows how the direction changes as the radius increases. The red curves in the bottom panel indicate the prediction of growth of the velocity of the Local Group for a WMAP5 cosmology. The solid curve gives the expectation of the reconstructed velocity for a survey whose radius is indicated by the X axis. The two dashed curve indicates the  $1\sigma$  fluctuation relative to the expectation given by the model. To compute these curves, we used the WMAP5 parameters: the density of cold dark matter  $\Omega_c = 0.212$ , the density of baryons  $\Omega_b = 0.044$ ,  $h = 0.719$ ,  $\sigma_8 = 0.77$  and a Eisenstein & Hu (1998) power spectrum (without baryonic wiggles).

universes whose cosmological parameters are selected by the likelihood analysis.

We use a  $\Lambda$ CDM power spectrum as given by Eisenstein & Hu (1998) but without incorporating baryonic wiggles. We have checked that introducing wiggles does not change the prediction much though the introduction of baryons does decrease the expectation of the reconstructed Local Group velocity for distances  $\lesssim 60h^{-1}$  Mpc. This behavior is expected as baryons tend to suppress density fluctuations below the sound horizon while they are linked to photons by the mean of the Compton effect. The size of the horizon at the moment when baryons separate from photons is typically  $\sim 45h^{-1}$  Mpc (Eisenstein & Hu 1998), which is the same scale at which we observe a change due to the introduction of baryons. In the presence of baryons the density

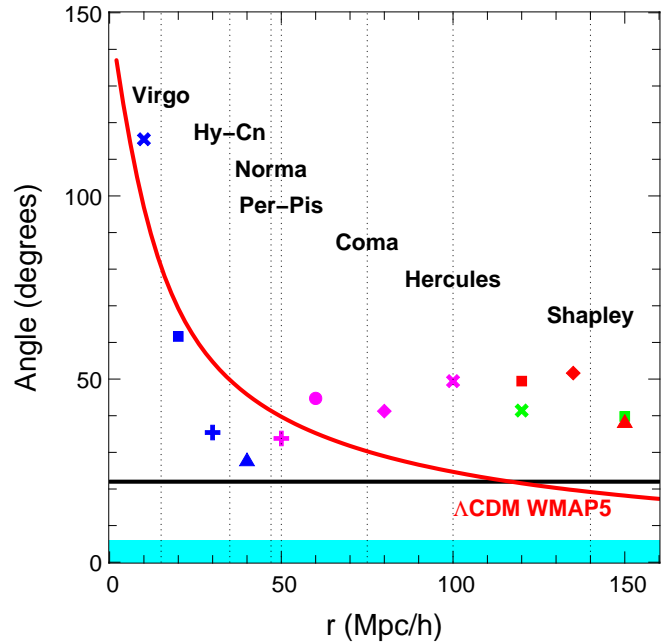


FIG. 5.— *Misalignment angle of the reconstructed Local Group velocity*— We have plotted here the misalignment angle between the reconstructed Local Group velocity and the direction indicated by the CMB dipole. The symbols and colors that are used here are the same as in Fig. 4. The red curve represents the 95% probability limit of the misalignment for a  $\Lambda$ CDM universe whose parameters have been chosen as estimated by WMAP5. The horizontal black thick line gives the expected misalignment, at 95% of probability, between the reconstructed velocity and the observed motion of the Local Group. It has been estimated by applying the reconstruction to one  $\Lambda$ CDM simulation.

field has less power on smaller scales, so it is more difficult for the Local Group to acquire its velocity using only small scale fluctuations. Fully computing the expected value of the Local Group velocity for a given survey depth, we indeed observe that it decreases by 5-15% when we take into account baryons in the power spectrum.

Now, we may also consider the effect of changing  $\sigma_8$ . Its principal effect is to change the amount of fluctuation of the velocity field around its expected value. A growth of convergence that is slow and regular corresponds most likely to a low local  $\sigma_8$ , whereas a growth with a lot of independent fluctuations favors a high  $\sigma_8$ . Its impact on the expectation of the amplitude of the velocity field is more complicated. Indeed, cosmologies with high  $\sigma_8$  tends to have stronger fluctuations relative to the expected velocity, which yields an higher expected amplitude. Thus higher  $\sigma_8$  should increase slightly the expectation of the amplitude. This means that even if we use only the evolution of the amplitude of the Local Group we should be sensitive to  $\sigma_8$ , though more marginally than on the shape of the power spectrum  $\Omega_m h$ . The impact of  $\sigma_8$  is however dominant concerning the fluctuations of the direction of the velocity of the Local Group. Only universes with a high  $\sigma_8$  allow this direction to depart significantly from the one given by the CMB dipole at scales larger than  $60h^{-1}$  Mpc as we will see in the section 6.1.

$\Omega_m$  represents the true dynamical content of the universe. For a given realization of density fluctuations, the dynamics is faster for a high  $\Omega_m$  than for a low  $\Omega_m$ . Thus

the convergence of the velocity of the Local Group should be quicker in a universe with a high  $\Omega_m$  than in another one with a low  $\Omega_m$ . But the expectation of this convergence does not tell anything about the probability on the velocity of the Local Group itself. We have decided in this work not to presume anything on the probability of occurrence of the velocity of the Local Group but only to check the consistency of the dynamics of the Local Universe.

We are now going to use the prediction of the growth of the Local Group velocity as both a checking of the  $\Lambda$ CDM model and a way to estimate cosmological parameters. We will explore a limited number of parameters: the total mean density of matter  $\Omega_m$ , the mean baryon density  $\Omega_b$ , the Hubble constant  $H$  and the variance  $\sigma_8$  of density fluctuations within a sphere of radius  $8h^{-1}$  Mpc.

In Section 6.1, we compare our results to predictions using WMAP5 cosmological parameters. In Section 6.2, we estimate cosmological parameters using both our measurements and the constraint coming from nucleosynthesis.

### 6.1. Comparison to WMAP5 results

First, we assume the  $\Lambda$ CDM model described above and we obtain the red curves represented in the bottom panel of Fig. 4. The solid curve gives the expectation of the convergence of the dipole given our motion. The dashed curves give the estimated  $1\sigma$  fluctuation for the expectation of the velocity of the Local Group for a given survey depth. This expectation is computed *assuming* that the Local Group is moving at  $627 \text{ km s}^{-1}$  relative to the CMB, as determined using CMB experiments. Though it seems astonishing to be systematically below the solid curve such a behavior may be explained by the fact that we are dealing with correlated measurements (see Section 6.2). For each point, the  $\Lambda$ CDM model seems to be in agreement with the Local Group velocity reconstructed by MAK at the  $1\sigma$  level. A similar prediction can be obtained for the maximum angle separation between the CMB dipole and the reconstructed velocity (equation 13). This prediction is represented by the solid red and thick curve in Fig. 5. For a given survey depth, the misalignment has a 95% probability to be located below the curve. This is in perfect agreement with the results given by the MAK reconstruction until a depth of  $60h^{-1}$  Mpc. There, the misalignment goes up to  $\sim 50^\circ$  and stays there. At  $100h^{-1}$  Mpc, we have a probability less than  $3 \times 10^{-5}$  that the misalignment is greater than  $50^\circ$ .

Given the importance of the disagreement between the predicted maximum misalignment and the observed one, we see three options. First, the reconstructed velocity of the Local Group may be exceptionally plagued by redshift distortions, even though on the rest of the volume the reconstructed velocity field is very well reconstructed. In this case, we are in the same position as number-weighted methods, which like in Erdoğdu et al. (2006a) yield a large misalignment. Doing a complete Monte-Carlo analysis on mock catalogs of these problems are beyond the scope of this paper, and we postpone this to future work. Second, we may miss some relatively important structures in the masked region. We remind that due to severe incompleteness we are miss-

ing information on structures below  $5^\circ$  for  $|l| > 30^\circ$  and  $10^\circ$  for  $|l| < 30^\circ$ . One of the brightest X-ray clusters of the Local Universe is the Ophiuchus Cluster at  $8400 \text{ km s}^{-1}$  and it may well reside in a hidden supercluster of significance (Wakamatsu et al. 2005). Second, more dramatically, it would mean that large bulk flows exist at a scale of  $100h^{-1}$  Mpc, typically  $\sim 500 \text{ km s}^{-1}$ . This is extremely unlikely in a  $\Lambda$ CDM cosmology as it is already highlighted by Fig. 5. A similar result has been obtained recently by Feldman et al. (2008) and Watkins et al. (2009) but using observed velocity fields. On the contrast, using linear theory on 2MRS (Erdoğdu et al. 2006a; Erdoğdu et al. 2006b) gives a low value of bulk flow and disagrees with Feldman et al. (2008) and Watkins et al. (2009).

### 6.2. Parameter estimation

From the measurements of the growth of the Local Group velocity, it is possible to estimate the joint probability of  $\Omega_m$  and  $\sigma_8$  by a maximum likelihood approach. To do that, we use a likelihood analysis on the velocity of the Local Group in the different rest frames that we obtained using 2MRS in Fig. 4. A similar analysis was first introduced by Kaiser & Lahav (1989) to compare predicted dipoles to observed bulk flows. Here, we focus on the expected evolution of the bulk flow on different scales and how it should compare to our own reconstructed bulk flow in a given cosmology. We detail, in Section 6.2.1, the statistics of the growth of the Local Group velocity using linear theory, an idea originally introduced by Juszkiewicz et al. (1990), Lahav et al. (1990) and Strauss et al. (1992). In Section 6.2.2, we see how to mix observational errors into this statistical modeling. Finally, in Section 6.2.3, we see the results of this analysis on the whole set of data points that we obtained on the value of the cosmological parameters.

#### 6.2.1. Statistics of the growth of the Local Group velocity

To estimate the likelihood of the cosmological parameter vector  $p$ , we need the conditional probability  $P(\mathbf{v}_1, \mathbf{v}_2, \dots, \mathbf{v}_N | \mathbf{V}_{\text{LG}}, p)$  of reconstructing the velocities of the Local Group  $\{\mathbf{v}_i\}$  in the set of rest frames  $\{\mathcal{R}_i\}$  given that the true velocity of the Local Group is  $\mathbf{V}_{\text{LG}}$  and the cosmological parameters are described by  $p$ . To estimate this probability, we will follow Juszkiewicz et al. (1990) and use linear theory and assume the components of the velocity field are independent Gaussian random variables. To ease the notation, we write  $\mathfrak{U}_k$  to designate the  $N$  dimensional vector whose  $i$ -th component is the  $k$ -th component of the  $i$ -th vector:  $\mathfrak{U}_{k,i} = (\mathbf{v}_i)_k$ . Using linear theory, we can compute the variance  $\sigma_i$  of the velocity of the Local Group computed using a homogeneously sampled spherical survey of depth  $R_i$

$$\sigma_i^2 = \frac{(\beta H)^2}{6\pi^2} \int_{k=0}^{+\infty} P(k) \widetilde{W}^2(kR_i) dk \quad (5)$$

with  $\widetilde{W}(x) = 1 - \sin(x)/x$ . We also define

$$\sigma_V^2 = \frac{(\beta H)^2}{6\pi^2} \int_{k=0}^{+\infty} P(k) dk \quad (6)$$

the variance of the velocity field. Similarly, one may obtain the correlation coefficient  $\gamma_{i,j}$  between the com-



ponent  $k$  of  $\mathbf{v}_i$  and  $\mathbf{v}_j$

$$\gamma_{i,j} = \frac{1}{\sigma_i \sigma_j} \langle v_{k,i} v_{k,j} \rangle = \frac{(\beta H)^2}{6\pi^2 \sigma_i \sigma_j} \int_{k=0}^{+\infty} P(k) \widetilde{W}(k R_i) \widetilde{W}(k R_j) dk \quad (7)$$

We also need the correlation  $\Gamma_i$  between  $v_{k,i}$  and  $V_{k,\text{LG}}$

$$\Gamma_i = \frac{1}{\sigma_i \sigma_V} \langle v_{k,i} V_{k,\text{LG}} \rangle = \frac{(\beta H)^2}{6\pi^2 \sigma_i \sigma_V} \int_{k=0}^{+\infty} P(k) \widetilde{W}(k R_i) dk. \quad (8)$$

We note that, even in the non-linear regime, the velocity field remains highly Gaussian. However, these coefficients do not take into account potential distortions to its correlations due to the MAK reconstruction and non-linear effects. Though, we expect the computation of these coefficients to be correct on large scales, precise measurements using  $N$ -body simulations would be required here to improve the precision on the final estimation of cosmological parameters when smaller scales are used. This measurement could be interesting as small scales may contain more information on  $\Omega_b$  and  $\sigma_8$ . Using these quantities it is now possible to compute the probability  $P(\mathbf{v}_1, \mathbf{v}_2, \dots, \mathbf{v}_N | \mathbf{V}_{\text{LG}}) = P(\vec{\mathfrak{U}} | \mathbf{V}_{\text{LG}})$ , with

$\vec{\mathfrak{U}} = (\mathfrak{U}_1, \mathfrak{U}_2, \mathfrak{U}_3)$ . We refer the reader to the appendix for the details of the computation. We carry here the result given in equation (A10):

$$P(\mathfrak{U}_k | V_{k,\text{LG}}) = \frac{\sqrt{\det M_s}}{(2\pi)^{N/2}} \prod_i \sigma_i^{-1} \times \exp \left( -\frac{1}{2} \sum_{i,j=1}^N \mathfrak{W}_{k,i} \mathfrak{W}_{k,j} M_{s,i,j} \right) \quad (9)$$

with

$$\mathfrak{W}_{k,i} = \frac{\mathfrak{U}_{k,i}}{\sigma_i} - \frac{\Gamma_i V_{k,\text{LG}}}{\sigma_V}. \quad (10)$$

and  $M_s$  the top-left part of the invert of the covariance matrix as defined in appendix by Eq. (A1). As the three components of the Local Group velocity are independent, the total probability of measuring the tensor  $\vec{\mathfrak{U}}$  given that the velocity of the Local Group is  $\mathbf{V}_{\text{LG}}$  is thus:

$$P(\vec{\mathfrak{U}} | \mathbf{V}_{\text{LG}}) = \prod_{k=1}^3 P(\mathfrak{U}_k | V_{k,\text{LG}}). \quad (11)$$

However, in Fig. 4, we see that errors coming from reconstructions are quite significant. We thus have to take them properly into account into the likelihood analysis.

### 6.2.2. Measurement errors

To account for reconstruction errors, we assume that they are independent from one survey depth to another and they are properly modeled by a Gaussian distribution. We will thus write the probability that the component  $k$  of the reconstructed velocity  $\mathbf{v}_{\text{rec},i}$  of the Local Group for a survey cut  $i$ , given that the true velocity should be  $\mathbf{v}_i$  for some cosmological model and the expected error dispersion for the component  $k$  is  $\sigma_{e,k,i}$ ,

$$P(v_{\text{rec},k,i} | v_{k,i}, \sigma_{e,k,i}) = \frac{1}{(2\pi)^{1/2} \sigma_{e,k,i}} \exp \left( -\frac{1}{2} \left( \frac{v_{\text{rec},k,i} - v_{k,i}}{\sigma_{e,k,i}} \right)^2 \right) \quad (12)$$

where  $v_{\text{rec},k,i} = (\mathbf{v}_{\text{rec},i})_k$  and  $v_{k,i} = (\mathbf{v}_i)_k$ . To ease the notation, we use now the  $N$ -dimensional vector  $\mathfrak{V}_k$ , whose components are  $\mathfrak{V}_{i,k} = (\mathbf{v}_{\text{rec},i})_k$ . So these vectors holds the component  $k$  of the reconstructed velocities for all survey depth.

We may now merge the two probabilities (9) and (12) to obtain the total probability to measure  $\mathfrak{V}_k$  given a cosmology determined by the vector of parameters  $p$  and the component  $k$  of the velocity of the Local Group  $V_{\text{LG},k}$ :

$$P(\mathfrak{V}_k | V_{\text{LG},k}, p) = \int_{\mathbf{U}} d\mathbf{U} \left( \prod_{i=1}^N P(v_{\text{LG},i,k} | U_i, \sigma_{e,i,k}) \right) P(U_1, U_2, \dots, U_N | V_{\text{LG},k}, p), \quad (13)$$

with  $\mathbf{U}$  a vector with  $N$  components. One may use a similar transformation as used in (A4) to compute the above integral and obtain the sought above probability:

$$P(\mathfrak{V}_k | V_{\text{LG},k}, \mathfrak{S}_{e,k}, p) = \frac{1}{(2\pi)^{N/2}} \sqrt{\frac{\det M_s}{\det M_{\text{obs}}(\mathfrak{S}_{e,k})}} \exp \left( -\frac{1}{2} f(\mathfrak{V}_k, V_{\text{LG},k}, \mathfrak{S}_{e,k}) \right) \quad (14)$$

where we defined the following quantities

$$f(\mathfrak{V}, V, \mathfrak{S}) = \sum_{i=1}^N \left( \frac{\mathfrak{V}_i - U_{\text{mean},i}}{\mathfrak{S}_i} \right)^2 + \sum_{i,j=1}^N \mathfrak{W}_{\text{mean},j} \mathfrak{W}_{\text{mean},i} M_{s,i,j}, \quad (15)$$

$$\mathfrak{W}_{\text{mean},i}(\mathfrak{V}, V, \mathfrak{S}) = U_{\text{mean},i}(\mathfrak{V}, V, \mathfrak{S}) / \sigma_i - \Gamma_i V / \sigma_V, \quad (16)$$

$$U_{\text{mean},i}(\mathfrak{V}, V, \mathfrak{S}) = \sum_{j=1}^N [M(\mathfrak{S})]_{\text{obs},i,j}^{-1} \left( \frac{\mathfrak{V}_j}{\mathfrak{S}_j^2} + \frac{V}{\sigma_V} \sum_{k=1}^N M_{s,j,k} \Gamma_k \right), \quad (17)$$

$$M_{\text{obs},i,j}(\mathfrak{S}) = M_{s,i,j} + \frac{\sigma_i^2 \delta_{i,k}}{\mathfrak{S}_i^2}. \quad (18)$$

It is interesting to note that  $U_{\text{mean},i}$  is a vector with  $N$  components which corresponds to the best average velocity given the cosmological model and observations. In some sense, it is a velocity whose observational noise has been subtracted thanks to the modeling. Finally, we may assemble the statistics of the three independent variable  $\mathfrak{V}_k$  with  $k = 1, 2, 3$ . We may do so by multiplying their respective probability distribution given by Eq. (14) to obtain

$$P(\mathbf{v}_1, \dots, \mathbf{v}_N | \mathbf{V}_{\text{LG}}, \sigma_{e,1}, \dots, \sigma_{e,N}, p) = \prod_{k=1}^N P(\mathfrak{V}_k | V_{\text{LG},k}, \mathfrak{S}_k, p). \quad (19)$$

We now use this probability and the Bayes theorem to compute the probability for the cosmological parameters  $p$

$$P(p | \mathbf{v}_1, \dots, \mathbf{v}_N, \mathbf{V}_{\text{LG}}, \sigma_{e,1}, \dots, \sigma_{e,N}) = \frac{P(\mathbf{v}_1, \dots, \mathbf{v}_N | \mathbf{V}_{\text{LG}}, \sigma_{e,1}, \dots, \sigma_{e,N}, p) P(p)}{\int_p dp P(\mathbf{v}_1, \dots, \mathbf{v}_N | \mathbf{V}_{\text{LG}}, \sigma_{e,1}, \dots, \sigma_{e,N}, p) P(p)} \quad (20)$$

with  $P(p)$  a prior on the probability of  $p$ . In practice, we use a flat prior on  $\Omega_m h^2$  and  $\sigma_8$  parameters and impose a prior on  $\Omega_b h^2$  and  $H$  as we detail in the next section.

### 6.2.3. Results

We set here a Gaussian prior on the Hubble constant to  $h = 0.72 \pm 0.08$  as specified by the HST Key project (Freedman et al. 2001) and the spectral index to  $n_s = 1$ . Nonetheless, we checked that the result depends only weakly on this prior. We also fix the observed velocity of the Local Group to  $V_{\text{LG}/\text{CMB}} = 627 \text{ km s}^{-1}$ . As we are using the power spectrum of Eisenstein & Hu (1998) without wiggles the cosmological parameter vector is thus  $p = (\Omega_m h^2, \Omega_b h^2, \sigma_8, h)$ . Note that the likelihood analysis, depending on the density power spectrum, should naturally depend on the shape  $\Omega_m h$  and not on  $\Omega_m h^2$ . On the other hand, WMAP5 data yield  $\Omega_m h^2$ , so we arbitrarily chose WMAP5 parametrization over the natural one. The expected growth of the Local Group velocity presents a substantial degeneracy in the  $(\Omega_m h^2, \Omega_b h^2)$  plane for scales smaller than the sound horizon ( $\sim 45 h^{-1} \text{ Mpc}$ ). To get better constraints, we need to introduce some prior on one of these two variable. Following the results obtained using the deuterium abundance (Pettini et al. 2008), we set a prior on  $\Omega_b h^2$  to a Gaussian distribution centered on  $\omega_b = \Omega_b h^2 = 0.0213$  and whose width is 0.0010:

$$P(p) \propto \exp \left( -\frac{1}{2} \left( \frac{\omega_b - 0.0213}{0.0010} \right)^2 \right), \quad (21)$$

with a constant of proportionality independent of  $p$ . We are not using the results from WMAP5 to make an independent comparison of their constraints and ours. We assume a flat prior on  $\omega_m = \Omega_m h^2$  and  $\sigma_8$  though we

---

enforce them to be within the ranges  $\omega_m \in [0, 1.0]$  and  $\sigma_8 \in [0.05, 7]$ .

The results given by Eq. (20) are illustrated in Fig. 6. In the left panel, the 68% (respectively 95% and 99.7%) isocontour of the marginalized joint probability of  $(\Omega_m h^2, \sigma_8)$  is represented in filled black (respectively dark gray and light gray) contour when all velocities up to  $100 h^{-1} \text{ Mpc}$  are taken into account. In the right panel, we represent the isocontours of probability when one considers only velocities up to  $60 h^{-1} \text{ Mpc}$ . The 68% (respectively 95%) probability for cosmological parameters using WMAP5 data alone are given by the hashed dark red (respectively hashed light red) filled contours in both panels.

It can be seen that our results in the right panel are compatible within  $1\sigma$  with WMAP5, as far as  $\omega_m$  and  $\sigma_8$  are concerned. However, in the left panel, the gray contours are significantly farther from WMAP5, though still within a  $2\sigma$  limit. This behavior is expected as we have already noticed that the misalignment angle does not seem to be compatible with a standard WMAP5 cosmology, though the growth of the amplitude is compatible. The introduction of points beyond  $\sim 60 h^{-1} \text{ Mpc}$  shifts the contours of probability to low  $\omega_m$  and high  $\sigma_8$ . A high  $\sigma_8$  allows strong fluctuation in the direction, thus increasing the expected amplitude, whereas a low  $\Omega_m$  limits the impact of these fluctuations on the amplitude of the velocity by making the convergence slower. At the same time these contours become smaller as the constraints are enforced by a larger number of data points. The analysis of all data points up to  $100 h^{-1} \text{ Mpc}$  shows that such a misalignment is less unlikely than what we would have expected from the observation of the curve of

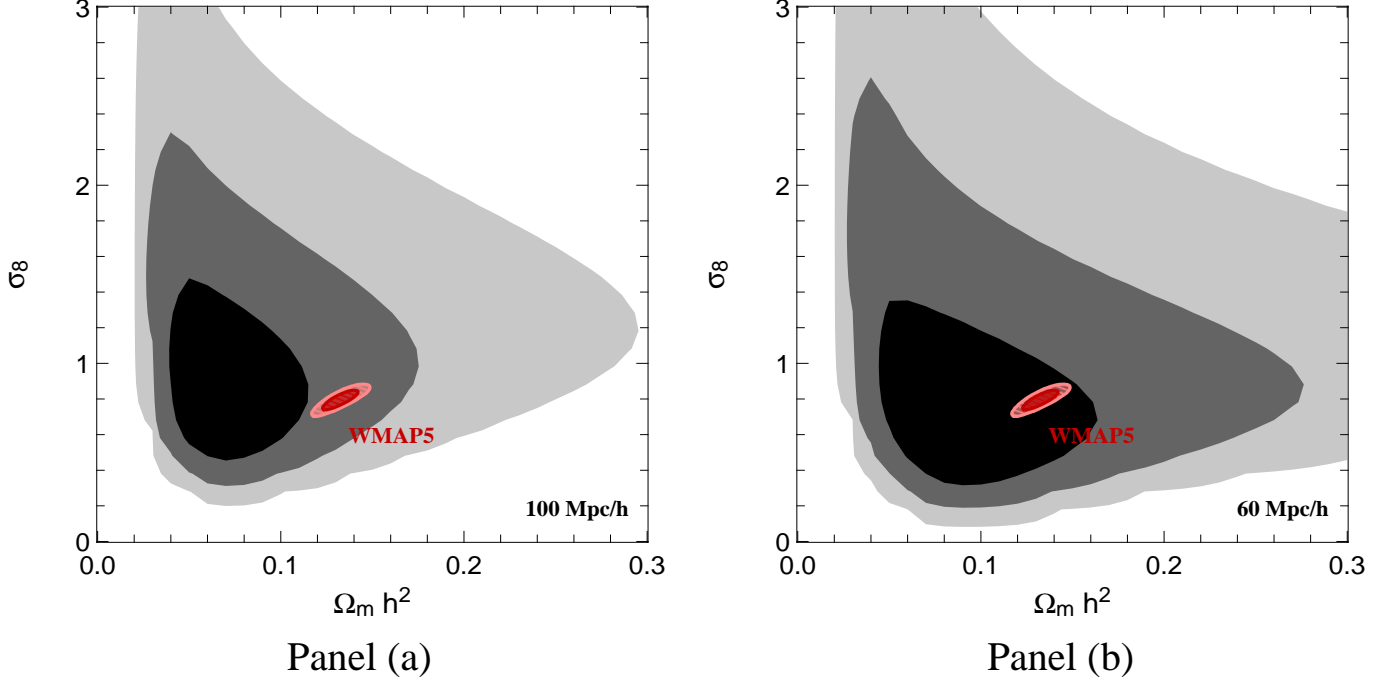


FIG. 6.— *Marginalized distribution of the joint probability of  $\Omega_m h^2 / \sigma_8$*  – In red, we represented the isocontour at 68% (dark red) and 95% (light red) of marginalized probability as given by WMAP5 (CMB data only). Left panel (a): We represented the isocontour at 68% (dark gray) and 95% of probability (light gray) as given by the likelihood analysis on the growth of the velocity of the Local Group up to  $100h^{-1}$  Mpc. For the gray contours, we introduced a prior on the mean density of baryons obtained by measuring the deuterium abundance (Pettini et al. 2008), which gives  $\Omega_b h^2 = 0.0213 \pm 0.0010$ . Right panel (b): The dark (68%) and light (95%) gray contours have been obtained in the same way as the gray contours of panel (a) except that we limited the depth of surveys to  $60h^{-1}$  Mpc inclusive.

Fig. 5. This can be explained by the fact the misalignment angles are not independent random variables. A more independent set of random variables would be the difference between the acceleration of the velocity the Local Group when one goes from one survey to a deeper survey. Thus, the strong misalignments of  $\sim 50^\circ$  for all  $R \geq 60h^{-1}$  Mpc, as we have on Fig. 5, might be generated by a single rare event within  $60 - 100h^{-1}$  Mpc from the observer which is not included in our present catalog, say a major supercluster in the Ophiuchus direction. The relative absence of matter in our catalog compared to the reality would push away the reconstructed velocity from the CMB direction, which corresponds to what we observe. We need to observe in greater detail the obscured part of the sky in these range of distances to resolve this issue. Another related reason for this misalignment might be an excessive mass in our model in the Perseus-Pisces supercluster. In the region delimited by a sphere of  $15h^{-1}$  Mpc centered on  $z=5000$  km s $^{-1}$ ,  $l = 140.2$ ,  $b = -22$ , we have put  $7.45 \times 10^{15} M_\odot$ . According to Hanski et al. (2001), this is on the high end of the expected mass of the Perseus-Pisces but not too excessive. A lower mass for this supercluster would push the velocity of the Local Group in the direction of the CMB.

We may check the adequacy of the conditional probability  $P(\vec{\mathcal{V}}|\mathbf{V}_{\text{LG}}, \vec{\mathcal{E}}, p)$  of reconstructing the set of Local Group velocities  $\vec{\mathcal{V}}$  given our observed motion  $\mathbf{V}_{\text{LG}}$  with the motion of the Local Group itself. To do that, we look at the total probability  $P(\vec{\mathcal{V}}, \mathbf{V}_{\text{LG}}|\vec{\mathcal{E}}, p) =$

$P(\vec{\mathcal{V}}|\mathbf{V}_{\text{LG}}, \vec{\mathcal{E}}, p) \times P(\mathbf{V}_{\text{LG}}|p)$ . We checked that in this case our results are not significantly affected, slightly moving the contours of both panels of Fig. 6 towards higher  $\omega_m$  and higher  $\sigma_8$ . This behavior is expected. This probability takes into account the fact that it is more likely to observe the velocity of the Local Group with respect to CMB in a denser universe and with larger density fluctuations. However, these considerations are insufficient to significantly change the computed contours.

On the contrary, we may relax the condition on the asymptotic reconstructed velocity, which is in principle given by the observed CMB dipole. In that case, we rely only on the evolution of the reconstructed velocities with the depth of the survey. Such an analysis shows the growth of the reconstructed velocity of the Local Group is compatible within  $1\sigma$ . However, this agreement is mainly due to the extension of the contours of probabilities of Fig. 6 because we do not enforce the observed motion of the Local Group. Doing so, we becomes less sensitive to potential large scale bulk flows and are unable to draw any meaningful conclusion about the cosmology.

To summarize, our results of this section indicate that, on one hand, the total matter density might be lower in the local Universe than that measured using WMAP5. On the other hand, the amount of fluctuation,  $\sigma_8$ , is more likely to be higher. Quantitatively, the maximum of the likelihood for the gray contours of the right panel is located at  $\omega_m \sim 0.08$  and  $\sigma_8 \sim 0.57$ . The mean of the gray distribution of the right panel are given by  $\Omega_m h^2 = 0.11 \pm 0.06$  ( $\Omega_m \sim 0.21 \pm 0.11$ ) and  $\sigma_8 = 0.90 \pm 0.42$ . For the gray contours of the left panel, this position is shifted



to  $\Omega_m h^2 = 0.08 \pm 0.03$  ( $\Omega_m \sim 0.15 \pm 0.06$ ) and  $\sigma_8 = 1.0 \pm 0.4$ . The most likely parameters are  $\omega_m = 0.090$  and  $\sigma_8 = 0.58$  for the right panel, and  $\omega_m = 0.070$  and  $\sigma_8 = 0.78$  for the left panel. We note that putting our estimate of  $\Omega_m$  of Section 4 and the above estimate of  $\omega_m$ , we may compute  $h \simeq 0.51$ , which is at odd with the estimate from the HST Key project. We expect some overlap at the low  $\omega_m$  and high  $\sigma_8$  part of the contour with Watkins et al. (2009). These discrepancies may be explained in three different manners. First, some more work on simulations are required to understand the potential systematics on these particular measures. Second, we know that there exists a large concentration of galaxies in the direction of the Ophiuchus at about  $80h^{-1}$  Mpc (Wakamatsu et al. 2005). This concentration is estimated to be as large as the Hercules supercluster and would need to be properly accounted in our statistical modeling as it is likely to systematically affect our reconstructed velocity. Third, we may live in a very special part of the Universe and we would thus need to go to larger scales using deeper catalogs to clarify this issue.

## 7. CONCLUSION

We have evaluated the 3-dimensional 2MRS peculiar velocity field using a Lagrangian method (MAK) which works well into the nonlinear regime, on scales above  $4.5h^{-1}$  Mpc. The method has been adapted to work directly with redshifts. The reconstructed velocities are well-correlated with the distances observed within a radius of  $3000 \text{ km s}^{-1}$  (3k sample). The reconstructed velocity of the Local Group in the rest frame of the 3k sample also agrees well with the observed value. In addition to this test, we have successfully compared the observed velocity field to the reconstructed ones within this same volume. This comparison has lead to an estimate of  $\Omega_m = 0.31 \pm 0.05$ .

We have then studied the origin of the Local Group motion in the CMB rest frame by using our 3d reconstructed velocities. We have shown that less than half of the CMB dipole could be generated within a radius enclosing the Hydra-Centaurus-Norma supercluster. We have demonstrated how the trend of the convergence varies up to  $120h^{-1}$  Mpc and have shown that convergence in position to the CMB dipole is not reached even by this distance.

We checked that our measurements of the amplitude are qualitatively in good agreement with the  $\Lambda$ CDM model for cosmological parameters given by WMAP5. We also note a weak dependence of the theoretical expectation of the amplitude on the presence of baryons that could be of interest to get better constraints if future work manages to reconstruct sufficiently well (at less than  $\sim 5\%$  error) the local dynamics. However, misalignment angles are significantly larger than anticipated by

the  $\Lambda$ CDM model on scales larger than  $50\text{--}60h^{-1}$  Mpc. To quantitatively check our measurements, we developed a Bayesian analysis of the growth of the velocity of the Local Group in the context of the linear theory but including correlations. We have shown that the growth of the velocity of the Local Group may be a powerful independent tool to explore cosmological parameters and of the dynamics of the Local Universe. This analysis yields an independent measurement of  $(\Omega_m h^2, \sigma_8)$  assuming the quantity of baryons using the nucleosynthesis theory. For scales up to  $60h^{-1}$  Mpc, our measurements agree with WMAP5 at the  $1\sigma$  level. For scales up to  $100h^{-1}$  Mpc, this agreement drops to 1 to  $2\sigma$ . This problem may have different origins: the incompleteness of the 2MRS, bad correction of redshift distortions at the introduction of the Perseus-Pisces or a real large bulk flow on the scale of  $\sim 100h^{-1}$  Mpc, which can represent a challenge for  $\Lambda$ CDM. More work on mock catalogs are needed to clarify this issue, which is beyond the scope of this paper.

Forthcoming deeper and more complete redshift surveys especially those in X-ray, could soon establish whether one has to go well beyond  $120h^{-1}$  Mpc to recover the CMB dipole or whether the Shapley concentration at around  $150h^{-1}$  Mpc is sufficient to finally reach the convergence. Such a larger survey would also allow a better comparison of our analysis of observations with the ones made on simulations on a similar scale to check  $\Lambda$ CDM features in the large scale velocity field, such as in Strauss et al. (1995).

## ACKNOWLEDGMENTS

We thank Joseph Silk for many enlightening suggestions. We thank the referee, Michael Hudson, for important contributions. We thank the 2MASS Redshift Survey collaboration for having kindly provided the observational data without which this study would not have been possible. G.L. and R.M. thank Michael Hudson and Jeremiah Ostriker for very helpful suggestions in particular on test of  $\Lambda$ CDM model. G.L., R.M. and B.T. acknowledge travel grants from French ANR (OTARIE). We thank S. Prunet, M. Chodorowski, T. Sousbie, E. Komatsu and O. Lahav for useful discussions. This publication makes use of data products from the Two Micron All Sky Survey, which is a joint project of the University of Massachusetts and the Infrared Processing and Analysis Center/California Institute of Technology, funded by the National Aeronautics and Space Administration and the National Science Foundation. This research was supported in part by the National Science Foundation through TeraGrid resources provided by the NCSA. TeraGrid systems are hosted by Indiana University, LONI, NCAR, NCSA, NICS, ORNL, PSC, Purdue University, SDSC, TACC and UC/ANL.

## REFERENCES

- Benjamin, J., Heymans, C., Semboloni, E., van Waerbeke, L. et al. 2007, MNRAS, 381, 702
- Branchini, E. & Plionis, M. 1996, ApJ, 460, 569
- Brenier Y., Frisch U., Hénon M., Loeper G. et al. 2003, MNRAS, 346, 501
- Cole, S., Percival, W. J., Peacock, J. et al. 2005, MNRAS
- Colless, M. 1995, AJ, 109, 1937
- Colombi, S., Chodorowski, M. J., & Teyssier, R. 2007, MNRAS, 375, 348
- Crook, A. C., Huchra, J. P., Martimbeau, N., Masters, K. et al. 2007, ApJ, 655, 790
- Crook, A. C., Huchra, J. P., Martimbeau, N., Masters, K. et al. 2008, ApJ, 685, 1320
- Davis, M. & Huchra, J. 1982, ApJ, 254, 437
- Dunkley, J., Komatsu, E., Nolte, M. R., Spergel D. N., et al. 2009, ApJS, 180, 306
- Eisenstein, D. J. & Hu, W. 1998, ApJ, 496, 605

TABLE 1  
THE RECONSTRUCTED CMB DIPOLE IN PROGRESSIVELY LARGER REST FRAMES  $R$

Observed velocity:  $V_{\text{LG/CMB}} = 627 \pm 22 \text{ km s}^{-1}$ ,  $l = 276 \pm 3$ ,  $b = 30 \pm 3$   
 $v_{\text{LG/CMB},x} = 56 \pm 28 \text{ km s}^{-1}$ ,  $v_{\text{LG/CMB},y} = -540 \pm 25 \text{ km s}^{-1}$ ,  $v_{\text{LG/CMB},z} = 313 \pm 30 \text{ km s}^{-1}$

$R$ ( $h^{-1}$ Mpc)	$V_{\text{LG/R}}$						
	$v_x$ ( $\text{km s}^{-1}$ )	$v_y$ ( $\text{km s}^{-1}$ )	$v_z$ ( $\text{km s}^{-1}$ )	$ V $ ( $\text{km s}^{-1}$ )	$l$ (deg)	$b$ (deg)	angular separation
20	$-157 \pm 71$	$-83 \pm 70$	$73 \pm 70$	192	207	22	62
30	$-122 \pm 71$	$-173 \pm 72$	$166 \pm 72$	269	234	38	35
40	$-137 \pm 71$	$-285 \pm 74$	$196 \pm 72$	372	244	31	27
50	$-172 \pm 72$	$-270 \pm 74$	$177 \pm 72$	365	237	29	34
60	$-236 \pm 73$	$-282 \pm 74$	$101 \pm 70$	382	230	15	45
80	$-208 \pm 72$	$-230 \pm 73$	$182 \pm 72$	360	228	30	41
100	$-328 \pm 76$	$-277 \pm 74$	$197 \pm 72$	473	220	25	49
120	$-378 \pm 78$	$-319 \pm 76$	$228 \pm 73$	544	220	25	49
150	$-257 \pm 74$	$-413 \pm 79$	$133 \pm 71$	504	238	15	38

NOTE – Glossary of the symbols used in the above tables.  $l$  and  $b$  are the galactic longitude and latitude respectively.  $R$  is gives the radius of the sub-volume of the catalog on which the reconstruction is achieved.  $v_i$  are the Cartesian galactic coordinates of the reconstructed velocity of the Local Group. The  $x$  axis points towards ( $l = 0, b = 0$ ), the  $y$  axis to ( $l = 90^\circ, b = 0$ ) and  $z$  to  $b = 90^\circ$ .

- Erdođdu, P., Huchra, J. P., Lahav, O., Colless, M., et al. 2006a, MNRAS, 368, 51
- Erdođdu, P., Lahav, O., Huchra, J. P., Colless, M., et al. 2006b, MNRAS, 373, 45
- Feldman, H. A., Hudson, M. J., & Watkins, R. 2008, Conference proceedings for the 43rd Rencontres de Moriond, ArXiv:0805.1721
- Freedman, W. L., Madore, B. F., Gibson, B. K., Ferrarese, L., et al. 2001, ApJ, 553, 47
- Fu, L., Semboloni, E., Hoekstra, H., Kilbinger, M. et al. 2008, A&A, 479, 9
- Giovanelli, R., Haynes, M. P., Wegner, G., da Costa, L. N., et al. 1996, ApJL, 464
- Hoffman, Y., Eldar, A., Zaroubi, S., & Dekel, A. 2001, arXiv preprint, astro-ph/0102190
- Hanski, M. O., Theureau, G., Ekholm, T., Teerikorpi, P. 2001, A&A, 378, 345
- Huchra, J. P. 2000, in ASPC series, Vol. 201, Cosmic Flows Workshop, ed. S. Courteau & M. Willick, 96
- Huchra, J. P., Martimbeau, N., Jarrett, T., Cutri, R., et al. 2005, in IAU Symposium, Vol. 216, Maps of the Cosmos, ed. M. Colless, L. Staveley-Smith, & R. A. Stathakis, 170
- Huchra, J. P. & Geller, M. J. 1982, ApJ, 257, 423
- Hudson, M. J. 1993, MNRAS, 265, 72
- Hudson, M. J. 1994, MNRAS, 266, 475
- Jackson, J. C. 1972, MNRAS, 156, 1P
- Juszkiewicz, R., Vittorio, N., & Wyse, R. F. G. 1990, ApJ, 349, 408
- Kaiser, N. 1987, MNRAS, 227, 1
- Kaiser, N. & Lahav, O. 1989, MNRAS, 237, 129
- Karachentsev, I. D., Makarov, D. I., Sharina, M. E., Dolphin, A. E., et al. 2003, A&A, 398, 479
- Kashlinsky, A., Atrio-Barendela, F., Kocevski, D., Ebeling, H. 2008, ApJL, 686, 49
- Kocevski, D. D. & Ebeling, H. 2006, ApJ, 645, 1043
- Lahav, O. 1987, MNRAS, 225, 213
- Lahav, O., Fabian, A. C., Edge, A. C., & Putney, A. 1989, MNRAS, 238, 881
- Lahav, O., Kaiser, N., & Hoffman, Y. 1990, ApJ, 352, 448
- Lahav, O., Lynden-Bell, D. & Rowan-Robinson, M. 1988, MNRAS, 234, 677
- Lauer, T. R. & Postman, M. 1994, ApJ, 425, 418
- Lavaux, G. 2009, in AIP proceedings serie, Invisible Universe International Conference, Paris, June 29-July 3, 2009, ed. J.-M. Alimi, ArXiv:0912.0516
- Lavaux, G., Mohayaee, R., Colombi, S., Tully B., et al. 2008, MNRAS, 383, 1292
- Lee, M. G., Freedman, W. L., & Madore, B. F. 1993, ApJ, 417, 553
- Lin, Y. T., Mohr, J. J., & Stanford, S. A. 2004, ApJ, 610, 745
- Lynden-Bell, D., Lahav, O., & Burstein, D. 1989, MNRAS, 241, 325
- Maller, A. H., McIntosh, D. H., Katz, N., & Weinberg, M. D. 2005, ApJL, 619, 147
- Massey, R., Rhodes, J., Leauthaud, A., Capak, P. et al. 2007, ApJS, 172, 239
- Mohayaee, R., Mathis, H., Colombi, S., Silk, J. 2006, MNRAS, 365, 939
- Mohayaee, R. & Tully, R. B. 2005, ApJL, 635, L113
- Muñoz, J. A. & Loeb, A. 2008, MNRAS, 391, 1341
- Pike, R. W. & Hudson, M. J. 2005, ApJ, 635, 11
- Pettini, M., Zych, B. J., Murphy, M. T., Lewis, A. et al. 2008, MNRAS, 391, 1499
- Plionis, M., & Kolokotronis, V. 1998, ApJ, 500, 1
- Ramella, M., Pisani, A., & Geller, M. J. 1997, AJ, 113, 483
- Regos, E. & Szalay, A. S. 1989, ApJ, 345, 627
- Rowan-Robinson, M., Lawrence, A., Saunders, W., Crawford, J. et al. 1990, MNRAS, 247, 1
- Rowan-Robinson, M., Sharpe, J., Oliver, S. J., Keeble, O. et al. 2000, MNRAS, 314, 375
- Scaramella, R., Baiesi-Pillastrini, G., Chincarini, G. Vettolani, G. et al. 1989, Nature, 338, 562
- Shaya, E. J., Peebles, P. J. E., & Tully, R. B. 1995, ApJ, 454, 15
- Skrutskie, M. F., Cutri, R. M., Stiening, R., Weinberg, M. D. et al. 2006, AJ, 131, 1163
- Strauss, M. A., Cen, R., Ostriker, J. P., Lauer, T. R. et al. 1995, ApJ, 444, 507
- Strauss, M. A., Huchra, J. P., Davis, M., Yahil, A. et al. 1992, ApJ, 83, 29
- Tegmark, M., Strauss, M. A., Blanton, M. R., Abazajian, K. et al. 2004, Phys. Rev. D, 69, 103501
- Tonry, J. & Schneider, D. P. 1988, AJ, 96, 807
- Tonry, J. L., Dressler, A., Blakeslee, J. P., Ajhar, E. A. et al. 2001, ApJ, 546, 681
- Tully, R. B. & Fisher, J. R. 1977, A&A, 54, 661
- Tully, R. B. & Pierce, M. J. 2000, ApJ, 533, 744
- Tully, R. B., Shaya, E. J., Karachentsev, I. D., Courtois, H. et al. 2008, ApJ, 676, 184
- Wakamatsu, K., Malkan, M. A., Nishida, M. T., Parker, Q. A. et al. 2005, in Astronomical Society of the Pacific Conference Series, Vol. 329, Nearby Large-Scale Structures and the Zone of Avoidance, ed. A. P. Fairall & P. A. Woudt, 189
- Watkins, R., Feldman, H. A., & Hudson, M. J. 2009, MNRAS, 392, 743
- Wegner, G., Bernardi, M., Willmer, C. N. A., da Costa, L. N. et al. 2003, AJ, 126, 2268
- Yahil, A., Sandage, A., & Tamman, G. A. 1980, ApJ, 242, 448
- Yahil, A., Walker, D., & Rowan-Robinson, M. 1986, ApJL, 301, 1
- Yahil, A., Strauss, M. A., Davis, M. & Huchra, J. P. 1991, ApJ, 372, 380
- Zel'dovich, Y. B. 1970, A&A, 5, 84

APPENDIX  
APPENDIX A

CONDITIONAL MULTIVARIATE GAUSSIAN RANDOM VARIABLES

We consider  $N + 1$  Gaussian random variables described by the vector  $(\mathbf{U}, V)$  with  $\mathbf{U}$  a vector of dimension  $N$  and  $V$  a scalar. In this appendix, we compute the statistics of  $\mathbf{U}$  given  $V$ . We put the normalized variables  $\hat{U}_i = U_i/\sigma_i$  and  $\hat{V} = V/\sigma_V$ . We assume that the correlation coefficients  $\gamma_{i,j} = \langle \hat{U}_i \hat{U}_j \rangle$  between the components  $U_i$  and  $U_j$  of  $\hat{\mathbf{U}}$  are given. We also assume that  $\Gamma_i = \langle \hat{U}_i \hat{V} \rangle$  is the correlation coefficient between  $\hat{V}$  and  $\hat{U}_i$ . The covariance matrix of this  $N + 1$  variables may thus be written as

$$C_{i,j} = \begin{cases} 1 & \text{if } i = j; \\ \gamma_{i,j} & \text{if } i \leq N \text{ and } j \leq N; \\ \Gamma_i & \text{if } i \leq N \text{ and } j = N + 1; \\ \Gamma_j & \text{if } i = N + 1 \text{ and } j \leq N. \end{cases} \quad (\text{A1})$$

We now write the invert of this matrix  $M = C^{-1}$  and  $M_s$  the top-left most  $N \times N$  sub-matrix of  $M$ . In other words, this sub-matrix corresponds to the first  $N$  lines and  $N$  columns of  $M$ . The probability of the vector  $(\hat{\mathbf{U}}, V)$  is thus:

$$P(\hat{\mathbf{U}}, \hat{V}) = \frac{1}{(2\pi)^{(N+1)/2} \sqrt{\det C}} \exp \left( -\frac{1}{2} {}^t \hat{\mathbf{U}} M_s \hat{\mathbf{U}} - \hat{V} M_{i,(N+1)} \hat{U}_i - \frac{1}{2} M_{(N+1),(N+1)} \hat{V}^2 \right). \quad (\text{A2})$$

Now we use Bayes theorem to compute  $P(\mathcal{U}|V)$ :

$$P(\mathcal{U}|\mathcal{V}) = \frac{P(\mathcal{U}, \mathcal{V})}{\int P(\mathcal{U}, \mathcal{V}) d\mathcal{U}}. \quad (\text{A3})$$

Before computing the integral in the denominator, we need to rewrite the argument of the exponential:

$${}^t \hat{\mathbf{U}} M_s \hat{\mathbf{U}} + 2 \hat{V} M_{i,(N+1)} \hat{U}_i + M_{(N+1),(N+1)} \hat{V}^2 = {}^t \hat{\mathbf{W}} M_s \hat{\mathbf{W}} + \alpha \hat{V}^2. \quad (\text{A4})$$

with

$$\hat{\mathbf{W}} = \hat{\mathbf{U}} + \hat{\mathbf{A}}, \quad (\text{A5})$$

$$\hat{A}_i = (M_s^{-1})_{i,j} M_{N+1,i} \hat{V} = -C_{N+1,i} \hat{V} = -\Gamma_i \hat{V}, \quad (\text{A6})$$

$$\alpha = M_{N+1,N+1} - M_{N+1,i} M_{s,i,j} M_{N+1,j}. \quad (\text{A7})$$

We may now compute the denominator:

$$\int_{\hat{\mathbf{U}}} P(\hat{\mathbf{U}}, \hat{V}) d\hat{\mathbf{U}} = \int_{\hat{\mathbf{W}}} \frac{\sqrt{\det M}}{(2\pi)^{(N+1)/2}} \exp \left( -\frac{1}{2} {}^t \hat{\mathbf{W}} M_s \hat{\mathbf{W}} - \frac{1}{2} \alpha \hat{V}^2 \right) = \frac{\sqrt{\det M}}{\sqrt{\det M_s}} \exp \left( -\frac{1}{2} \alpha \hat{V}^2 \right). \quad (\text{A8})$$

We may rewrite the argument of the exponential in the numerator using (A4) and deduce the conditional probability

$$P(\hat{\mathbf{U}}|\hat{V}) = \frac{\sqrt{\det M_s}}{(2\pi)^{N/2}} \exp \left( -\frac{1}{2} (\hat{U}_i - \Gamma_i \hat{V})(\hat{U}_j - \Gamma_j \hat{V}) M_{s,i,j} \right). \quad (\text{A9})$$

This conditional probability is written in terms of the normalized variables  $\hat{\mathbf{U}}$  and  $\hat{V}$ . The probability may be rewritten in terms of the original random variables by an appropriate change of variables:

$$P(\mathbf{U}|V) = \frac{\sqrt{\det M_s}}{(2\pi)^{N/2}} \left( \prod_{i=1}^N \frac{1}{\sigma_i} \right) \exp \left( -\frac{1}{2} (U_i/\sigma_i - \Gamma_i V/\sigma_V)(U_j/\sigma_j - \Gamma_j V/\sigma_V) M_{s,i,j} \right). \quad (\text{A10})$$

APPENDIX B

COMPARISON OF LINEAR THEORY AND MAK RECONSTRUCTION OF DIPOLE

We have demonstrated, in contrast to previous reconstruction of 2MRS peculiar velocities (Erdoğdu et al. 2006a; Erdoğdu et al. 2006b), that our method agrees well with recent works which make direct use of observed peculiar velocities (Feldman et al. 2008). In this appendix, the difference between linear theory and MAK determination of bulk flow is studied.

There are mainly two ways of implementing linear theory for getting the velocity of the Local Group. One method is the flux-weighted method (as recently done for 2MRS in Erdoğdu et al. 2006a). The second method uses linearized



TABLE 2  
STRUCTURES PROBED FOR COMPARING WITH LINEAR THEORY

Structure	$z_{\min}$ (km s <sup>-1</sup> )	$z_{\max}$ (km s <sup>-1</sup> )	$l$ (deg)	$b$ (deg)	Opening angle (deg)
Virgo	no minimum	3000	279	74	20
Hydra	2000	4300	269	26	15
Centaurus	2000	4300	302	21	15
Perseus-Pisces	4000	6000	150	-13	20
Fornax	no minimum	1600	240	-50	20

TABLE 3  
IMPACT OF STRUCTURES ON THE FINAL VELOCITY OF THE LOCAL GROUP, SMOOTHED WITH A GAUSSIAN KERNEL OF  $5h^{-1}$  MPC RADIUS

Method	Structure (S)	Mass (M <sub>⊙</sub> )	$\delta\mathbf{v}_{S,\text{method}}$		
			$ \delta V $ (km s <sup>-1</sup> )	$l$ (deg)	$b$ (deg)
MAK	Virgo	$1.3 \times 10^{15}$	89	302	88
Linear			230	297	68
MAK	Fornax	$3.6 \times 10^{14}$	52	261	-15
Linear			94	271	-1
MAK	Hydra-Centaurus	$4.3 \times 10^{15}$	88	281	35
Linear			189	297	39
MAK	Perseus-Pisces	$8.9 \times 10^{15}$	105	167	10
Linear			52	139	48

*Note* – We are giving in this table the direction and amplitude of the velocity vector corresponding to the velocity of the Local Group when all structures are present minus its velocity when we removed the indicated structure. The structures are defined in Table 2. The comparison is done for both the result given by MAK and the linear theory.

fluid equation to infer the velocity field from the density field. The advantage of the former method is that it bypasses the redshift space distortions, which could be problematic for objects highly extended in redshift space (e.g. Virgo cluster). The disadvantage of this method is that it is limited to the velocity of the Local Group. It does not yield the peculiar velocity field and especially in the local neighborhood. In addition, to study the impact of farther and farther structures on the Local Group, one often substitutes distances by redshifts.

The second way of obtaining peculiar velocity field from linear theory relies on linearized fluid equations. The disadvantage of this method is that the Local Group velocity becomes sensitive to redshift space distortions. The advantage is that we obtain the 3d velocity field everywhere and not just at our location. In this appendix, we compare this way of implementing linear theory with MAK.

To estimate the velocity of the Local Group with linear theory, we follow the same procedure for accounting for redshift distortions as for MAK, except that we use the linear relation between peculiar velocity field and the density field given by:

$$\text{div } \mathbf{v} = -\beta H \delta, \quad (\text{B1})$$

where  $\beta = \Omega_m^{5/9}/b$ ,  $b$  is the bias,  $H$  the Hubble constant and  $\delta$  the density fluctuations. We use a Gaussian smoothing filter of  $2.5h^{-1}$  Mpc of radius and increase progressively  $\beta$  to increase numerical stability (e.g Pike & Hudson 2005).

To study the difference between linear theory and MAK, we look at four most prominent structures (listed in Table 2) in 2MRS catalog and study their effect on the Local Group motion. We evaluate the Local Group velocity in the presence and in the absence of these four structures using both linear theory and MAK. We computed the velocity of the Local Group based on a  $60h^{-1}$  Mpc cut of the 2MASS Redshift Survey and in the rest frame of this volume.

Table 3 demonstrates the effect of these four structures on the Local Group velocity. We note that linear theory overestimates the Local Group motion due to lower mass nearby objects and underestimates the effect of high mass farther objects. This deserves a full theoretical understanding in the framework of perturbative theory which is beyond the scope of this work. Since Perseus-Pisces is the most massive object in our study, we also show in Figure 7 the effect of this structure on the entire velocity field, as reconstructed using linear theory and MAK. The large scale flows are similar in the two methods and, as expected, the small scale flows are different.

We have done a more extensive test of the difference between linear theory and MAK reconstruction through a Monte-Carlo test. We have taken fifty observers, randomly located in the simulation, and built a mock catalog centered on each of these observers. These mock catalogs are extracted from the  $\Lambda$ CDM simulation described in Lavaux et al. (2008). Each mock catalog is limited in depth to  $60h^{-1}$  Mpc and mock galaxies and groups are put in redshift space. We calculated the velocity of the mock observer given by the linear theory and by MAK and then compared these to the true value given by the simulation. The result is shown in Figure 8. MAK presents a dispersion  $\sim 30\%$  less than linear theory. (For other comparisons with linear theory see Lavaux 2009.)

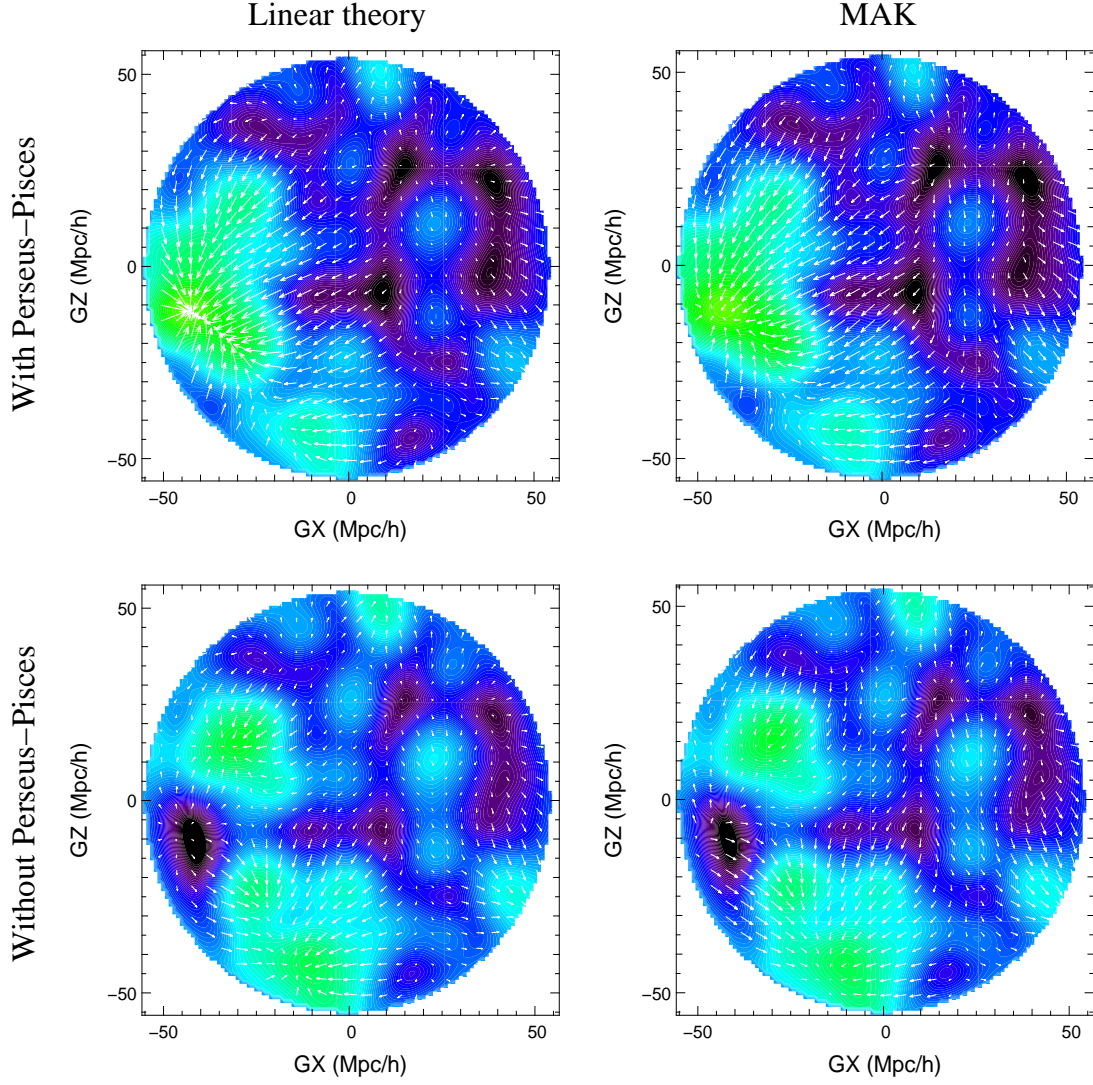


FIG. 7.— *Reconstructed velocity field in the region of the Perseus-Pisces in Galactic coordinates* – We give here the reconstructed velocity field using either linear theory (left panels) or by solving the Monge-Ampère-Kantorovitch problem (right panels) for two cases: with the Perseus-Pisces supercluster (top row), and removing the galaxies of the Perseus-Pisces supercluster (bottom row). In all cases, we limited the reconstruction to a volume of radius  $60h^{-1}$  Mpc from the observers. The slice is centered on the Perseus cluster and does not contain Milky Way. The slice corresponds actually to  $GY=25h^{-1}$  Mpc.

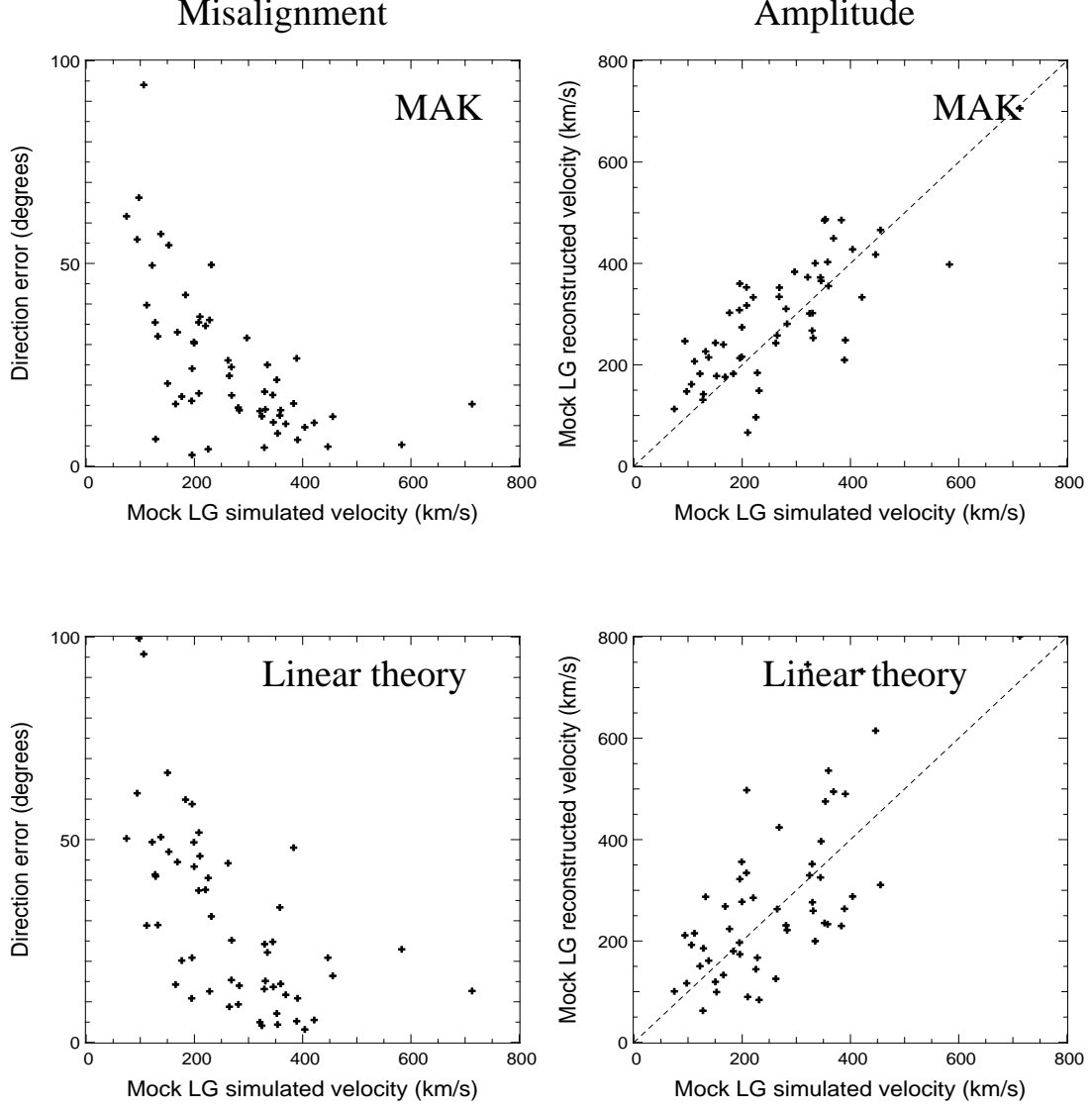


FIG. 8.— *Comparing MAK to linear theory through Monte Carlo tests: reconstructed velocity vs. simulated velocity* – We represent here the comparisons between reconstructed velocities (top row MAK and bottom row linear theory) and simulated velocities of 57 mock-observers in 57 mock catalogs. The velocity fields (simulated, reconstructed by MAK, reconstructed by linear theory) were smoothed to  $2.5h^{-1}$  Mpc with a Gaussian kernel. Left panels: direction misalignment vs amplitude of the simulated velocity. Right panels: amplitude of the reconstructed velocity vs amplitude of the simulated velocity. The mock-observer velocities reconstructed using MAK (top row) show  $\sim 30\%$  less dispersion with respect to linear theory.



## APPENDIX C

## ADAPTIVE SMOOTHED INTERPOLATION

We make use of a technique inspired from adaptive smoothing (Colombi et al. 2007), while changing the weight such that we make an smoothed interpolation of the required field (in this work the velocity field). We put  $A(\mathbf{y})$  the underlying continuous field, and  $A_i$  its value at the position  $\mathbf{x}_i$ . We now define the smoothed interpolated field

$$\tilde{A}(\mathbf{y}) = \frac{1}{N(\mathbf{y})} \sum_{i=1}^M W\left(\frac{\mathbf{y} - \mathbf{x}_i}{R(\mathbf{y})}\right) A_i \quad (\text{C1})$$

with  $M$  the number of tracers on which the smoothed interpolation is done,

$$N(\mathbf{y}) = \sum_{i=1}^M W(\mathbf{y} - \mathbf{x}_i) \quad (\text{C2})$$

the normalization coefficient of the smoothing and

$$W(x) = \begin{cases} 1 - \frac{3}{2}x^2 + \frac{3}{4}x^3 & x \leq 1 \\ \frac{1}{4}(2-x)^2 & 1 < x \leq 2 \\ 0 & \text{otherwise} \end{cases} \quad (\text{C3})$$

the smoothing kernel used. In practice, in the above smoothing procedure, we set  $M = 32$ , and  $R(\mathbf{y})$  is half the distance to the 32-th neighbors from  $\mathbf{y}$ .

It can be shown that for class 1 function<sup>5</sup> and an unbiased distribution of tracers of  $A(\mathbf{y})$  this smoothing procedure converges normally on any volume  $V$ . Locally, the sum (C1) may be expanded in

$$\tilde{A}(\mathbf{y}) = \frac{1}{N(\mathbf{y})} \sum_{i=1}^M W\left(\frac{\mathbf{y} - \mathbf{x}_i}{R(\mathbf{y})}\right) (A(\mathbf{y}) + (\nabla A)(\mathbf{y}) \cdot (\mathbf{x}_i - \mathbf{y})) \quad (\text{C4})$$

$$= A(\mathbf{y}) + (\nabla A)(\mathbf{y}) \cdot \left( \sum_{i=1}^M \frac{1}{N(\mathbf{y})} W\left(\frac{\mathbf{y} - \mathbf{x}_i}{R(\mathbf{y})}\right) (\mathbf{x}_i - \mathbf{y}) \right). \quad (\text{C5})$$

The second term on the right-hand-side may be bound by:

$$(\nabla A)(\mathbf{y}) \cdot \left( \sum_{i=1}^M \frac{1}{N(\mathbf{y})} W\left(\frac{\mathbf{y} - \mathbf{x}_i}{R(\mathbf{y})}\right) (\mathbf{x}_i - \mathbf{y}) \right) \leq 2 \|\nabla A\|_{+\infty, V} M R. \quad (\text{C6})$$

As  $R \propto n^{-1/3}$  with  $n$  the number density of tracers and that  $\|\nabla A\|_{+\infty}$  is bounded on any volume  $V$ , the above quantity decreases to zero when  $n \rightarrow +\infty$  and the interpolation  $\tilde{A}$  converges to  $A$ .

## APPENDIX D

TEST OF 2MRS RECONSTRUCTED VELOCITIES WITH OBSERVED DISTANCES WITHIN 3,000 km s<sup>-1</sup>

The reconstructed velocities of objects lying only within the 3,000 km s<sup>-1</sup> radius can be compared to the measured distances given by the 3k distance catalog (Tully et al. 2008). The measured distances give a velocity of the Local Group with respect to the 3,000 km s<sup>-1</sup> volume of  $V_{\text{LG}/3\text{k}} = 302 \pm 22$  km s<sup>-1</sup>,  $l = 241 \pm 7$ ,  $b = 37 \pm 6$ . The observation indicates that most of this velocity comes from the push from the Local Void and the gravitational pull of the Virgo cluster (Tully et al. 2008). The velocity of the Local Group with respect to the 3,000 km s<sup>-1</sup> volume ( $V_{\text{LG}/3\text{k}}$ ) is obtained using our reconstructed 2MRS velocities. The reconstructed  $V_{\text{LG}/3\text{k}}$  is compared with the observed value in Fig. 9. The coordinates of the reconstructed dipoles are given in Table 4. The influence of other structures, like the Hydra-Centaurus-Norma at 40-50  $h^{-1}$  Mpc, seems marginal in this rest frame. So we conclude that the reconstruction indeed shows that the  $V_{\text{LG}/3\text{k}}$  motion seems mainly generated within the 3,000 km s<sup>-1</sup> volume.

<sup>5</sup> Class 1 functions are continuous and their derivative is also continuous.

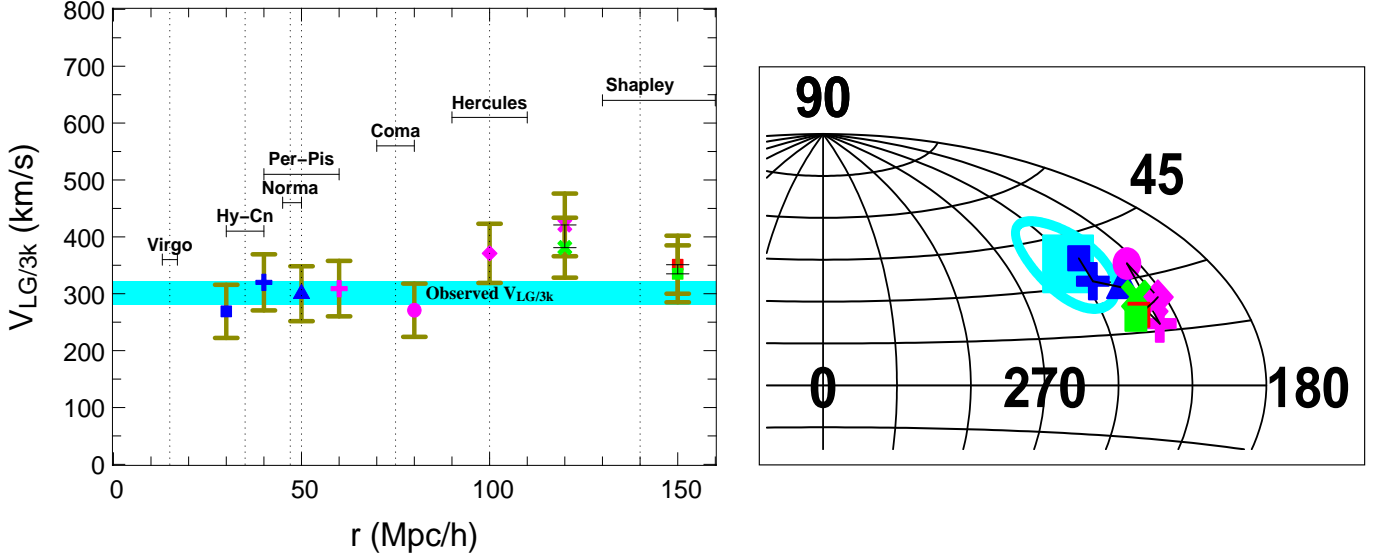


FIG. 9.— *The origin of motion of the Local Group in the rest frame of galaxies in the  $3,000 \text{ km s}^{-1}$  ( $3k$ ) volume,  $V_{LG/3k}$ :* The observed amplitude and direction of the  $V_{LG/3k}$  are shown by the horizontal cyan band in the lower panel and the solid cyan large square in the top panel, respectively. The observational error on the direction is shown on the top panel by the thick cyan ellipse. Each reconstructed point is affected by a  $22^\circ$  error. The reconstructions indicate that most of the motion is generated by the structures within this volume, in agreement with the observations. It is seen that most of the motion is generated within  $3,000 \text{ km s}^{-1}$ . The jump at around  $120h^{-1} \text{ Mpc}$  is most probably caused by the severe incompleteness of 2MRS at this distance. The represented error bar have been computed by adding in quadrature the 9% systematic error bar due to the uncertainty on  $\Omega_m$  and a random reconstruction error of  $70 \text{ km s}^{-1}$ . Incompleteness results in uncertainties illustrated by the black error bars on data points beyond  $120h^{-1} \text{ Mpc}$  in the bottom panel.

TABLE 4

COMPARISON BETWEEN THE OBSERVED AND THE RECONSTRUCTED VELOCITY OF THE LOCAL GROUP IN THE  $3,000 \text{ km s}^{-1}$  REST FRAME

Observed velocity:  $V_{LG/3k} = 302 \text{ km s}^{-1}$ ,  $l = 241$ ,  $b = 37$

$v_{LG/3k,x} = -125 \pm 24 \text{ km s}^{-1}$ ,  $v_{LG/3k,y} = -210 \pm 21 \text{ km s}^{-1}$ ,  $v_{LG/3k,z} = 181 \pm 18 \text{ km s}^{-1}$

$R_{\text{rec}}$ ( $h^{-1} \text{ Mpc}$ )	$V_{LG/3k}$				$l$ (deg)	$b$ (deg)	angular separation
	$v_x$ ( $\text{km s}^{-1}$ )	$v_y$ ( $\text{km s}^{-1}$ )	$v_z$ ( $\text{km s}^{-1}$ )	$ V $ ( $\text{km s}^{-1}$ )			
30	$-122 \pm 71$	$-173 \pm 71$	$166 \pm 71$	269	234	38	5
40	$-150 \pm 71$	$-228 \pm 73$	$166 \pm 71$	320	236	31	7
50	$-183 \pm 72$	$-187 \pm 72$	$145 \pm 71$	300	225	28	16
60	$-232 \pm 73$	$-182 \pm 72$	$90 \pm 70$	309	218	17	28
80	$-183 \pm 72$	$-128 \pm 71$	$154 \pm 71$	271	215	34	21
100	$-282 \pm 73$	$-176 \pm 72$	$152 \pm 71$	371	213	24	27
120	$-311 \pm 73$	$-230 \pm 73$	$164 \pm 71$	421	216	23	25
150	$-231 \pm 73$	$-234 \pm 73$	$124 \pm 71$	351	225	20	21